Toward representing the subsurface nitrate legacy through a coupled StorAge Selection function and hydrological model (SWAT-SAS)

Wuhua Li[1,2,*], Tam V. Nguyen[3], Xiangju Cheng[1,4,*], Dantong Zhu[1,4], Rohini Kumar[2,*]

[1] School of Civil Engineering and Transportation, South China University of Technology, Guangzhou, China

[2] Department of Computational Hydrosystems, Helmholtz Centre for Environmental Research – UFZ, Leipzig, Germany

[3] Department of Hydrogeology, Helmholtz Centre for Environmental Research – UFZ, Leipzig, Germany

[4] State Key Laboratory of Subtropical Building Science, South China University of Technology, Guangzhou, China

[*] Corresponding author

Abstract

The transit time distribution (TTD) is a lumped method to characterize the diverse flow paths of a hydrological system, and the StorAge Selection function (SAS) is one of the time-variant forms, representing the link between storage and outflow. Although it provides age information about the water parcels and nutrient legacy, the spatial heterogeneity cannot be captured by this method. While the distributed physically-based hydrological models (PBHMs) can reflect the spatial heterogeneous in climate, land cover and management, its simplification of subsurface processes prevents it from representing the subsurface nutrient transport and sometimes fails to capture nutrient legacy dynamics of the landscape. We attempted to couple SAS functions into a PBHM (SWAT) for calculating the nitrate dynamics of aquifers. The results show that both SWAT-SAS and SWAT can reproduce the in-stream dynamics of streamflow and nitrate concentration for the Upper Selke catchment; the coupled model allows more flexibility of storage release schemes and provides water age information of the aquifers; even though both the models simulated comparable

in-stream nitrate concentrations, the nitrate store remained in aquifers varied, which will have varying implications for pollution goal assessment and nutrient management.

Keywords: Hydrological model, SWAT, StorAge Selection function, Transit time distribution, Nutrient transport

1 Introduction

Despite years of action and reductions in nitrogen (N) emissions, N pollution levels have not achieved the expected results (Basu et al., 2022). The perplexing occurrences are widespread and pose significant challenges to resource conservation, watershed management and adaptation to climate change (Basu et al., 2022; Meter et al., 2018; Van Vliet et al., 2023). Recent studies have suggested that neglecting the N legacy store in the landscape is one of the key drivers of the failure cases (Basu et al., 2022; McDowell et al., 2021). It has also been estimated that a significant portion of N is retained in the catchment for years or even decades (Ehrhardt et al., 2021), and the lag time between management and riverine response would vary according to factors like slope and hydroclimate (McDowell et al., 2021). Many geochemical observations of conservative tracers have reported the “old water paradox,” emphasizing the contribution of previously stored water to the streamflow in response to rainfall inputs. Either the obstacle to improving water quality caused by the N legacy or the mismatch between inputs and outputs during the storm events is related to the transport pathways within the catchment. At present, linking the water flow and solute transport in a comprehensive framework remains a challenge due to the spatial and temporal heterogeneity of the hydrologic system, data scarcity, and model limitation, but is essential for understanding the biogeochemical processes, predicting the hydrologic response, environmental assessment, and resource management (Blöschl et al., 2019). The standard metrics (e.g., flow, water level, and solute concentration) are not sufficient to support hydrologists in unrevealing the “black box” of subsurface processes, and the transit time concept is emerging as a common method to represent both flow and transport (Benettin et al., 2022).

Transit time (TT) is the time it takes for a water parcel to travel through a catchment. By tagging the water parcels with “time stamps,” the complex three-dimensional flow path is simplified by a one-dimensional descriptor and the age of a water parcel suggests how long it takes for the water parcel to reach the outlet. The transit time distribution (TTD) is the probability density function of TT for ensemble water parcels, which is an integrated descriptor to characterize the statistical properties of diverse flow paths. TTDs connect to the process complexity of a catchment, indicating how the catchments retain and release water and solutes (Botter et al., 2011; McGuire et al., 2007; McGuire and McDonnell, 2006; Rinaldo et al., 2015).

In early work, the TTDs of hydrologic systems were generally assumed to have a prior form (e.g., gamma distribution and exponential distribution) and the parameters are estimated through tracer experiments (Kirchner et al., 2000; Maloszewski and Zuber, 1993, 1982; McDonnell et al., 2010; McGuire and McDonnell, 2006; Niemi, 1977; Rinaldo and Marani, 1987). However, hydrologic systems are typically heterogeneous in space and time, including the internal changes in flow paths, soil moisture and hydraulic conductivities, as well as the external aspects of meteorological conditions and surface variability. For the former, the TTD theory needs to be developed to reflect the dynamics of internal processes. As demonstrated by many tracer experiments and simulations, the TTD should be time-variant to reflect arbitrary input forcings and related process dynamics (Botter et al., 2011, 2010; Harman, 2015; Heidbüchel et al., 2013; Hrachowitz et al., 2010; Rodriguez et al., 2019; Velde et al., 2012). The StorAge Selection (SAS) function is one of the new models and approaches introduced in recent years, which can be employed in a time-variant system (Botter et al., 2011; Rinaldo et al., 2015). Instead of formulating the TTD directly, the SAS function links relationship between the storage and outflow, representing how the storage is selected and contributes to discharge (Harman, 2015). SAS function is mathematically parsimonious and flexible to describe different transport behaviors of the system with only a few parameters. It is becoming a hot spot for transit time modeling (Meira Neto et al., 2022; Nguyen et al., 2021, 2022b; Rinaldo et al., 2015) in various scales and areas including bench-scale experiments (Meira Neto et al., 2022), hillslope landscape (Kim et al., 2022), deep valley (Rodriguez et al., 2021), agricultural catchment (Dupas et al., 2020), lowland catchment (Velde et al., 2010), mesoscale catchment (Nguyen et al., 2021, 2022b) and some complex areas such as karst area (Z. Zhang et al., 2020; Zhang et al., 2021). However, time-variant TTDs such as SAS function are lump-parameter methods and still cannot capture the spatial heterogeneity. Although the variant rainfall data can be input into the models, the spatial distribution of geomorphology and land cover, which might significantly influence the hydrological processes and further the in-stream hydrographs, are not well represented in this approach.

The distributed Process-based hydrological model (PBHM) provides clear physical meaning and considers both spatial distribution complexity and process complexity, allowing it to represent the heterogeneity of climate and land cover, as well as the processes within landscapes and channels. Some attempts have been made to infer transit times from the fully distributed PBHM, and subsequently to improve the matter transport representation. For example, the MIPs (Multiple Interacting Pathways) framework (Davies et al., 2013), the WATET (Water Age and Tracer Efficient Tracking) based on TOPKAPI-ETH (Remondi et al., 2018), Eco-Silm (Maxwell et al., 2019), ParFlow-SLIM methods (Danesh-Yazdi et al., 2018; Engdahl and Maxwell, 2015), the NIHM-based model (Weill et al., 2019) and mHM-OGS (Jing et al., 2021). However, these methods are data-intensive, and more data and greater computational resources are required for large study areas. In addition, implementing fully distributed PBHMs in real-word scenarios faces challenges in terms of scale effect, parameterization difficulties, and limited applicability of watershed management.

With the increasingly significant impact of anthropogenic activities and climate change on human society and ecosystems, simulating the hydrological and water quality effects under changing environments is of great necessity for water resources protection and watershed management. The semi-distributed PBHMs such as SWAT and HSPF have provided good considerations in spatial heterogeneity and discretization calculation, which have been successfully applied in various scales of catchments. However, the solute transport model of these models has been noted to have limitations in representing subsurface heterogeneity. Some research and models make a difference by introducing retention/passive storage, more detailed flow mechanisms or new parameters to improve the chemical response (Hrachowitz et al., 2013; Renée Brooks et al., 2010; X. Yang et al., 2018). These methods also introduce much uncertainty, and the model might become bulky for more complicated areas. A unified theory is needed to generalize the transport processes beneath the surface (Hrachowitz et al., 2016; Kirchner, 2003; Lutz et al., 2022). Recently, there has been an increasing awareness of using transit time information for water quality models (Benettin et al., 2022; Fu et al., 2019; Hrachowitz et al., 2016; Rinaldo et al., 2015). The TTD/SAS concepts have been successfully implemented in water quality models for hillslope scale (Kim et al., 2022), mesoscale catchments (Nguyen et al., 2022a, 2021), lakes (A. A. Smith et al., 2018) and catchments with strong seasonality (Yang et al., 2021), improving the process representation as well as giving physically interpretation of the results.

Here, we propose to couple the SAS function into a semi-distributed PBHM, allowing the coupled model to consider the spatial heterogeneity of the land cover with improved subsurface solute transport representation. The semi-distributed PBHM employed was the SWAT (Soil and Water Assessment Tool), which has developed for several decades and widely used in many areas. Daily discharge and nitrate concentrations simulated by the coupled model (hereafter called SWAT-SAS) were compared with the original SWAT model. Our objectives are: (1) modify SWAT for simulating the aquifer nitrogen transport with SAS functions, (2) compare the results of the modified model and the original model, and (3) highlight the additional information that SWAT-SAS provided and its potential for supporting contamination treatment and watershed management.

2 Methodology

2.1 SWAT model description

SWAT (Soil and Water Assessment Tool) is a continuous time, semi-distributed hydrological model at the watershed scale with a strong physical mechanism (Arnold et al., 2012, 1998). SWAT defines watershed boundaries according to topography and then delineates streams and subbasins. Considering the spatial heterogeneity of land use, soil, and slope, subbasins are further discretized into individual hydrological response units (HRUs). The HRU is the smallest computational unit of the model, simulating processes such as hydrology, sediment, nutrients, management, etc. The HRU results will be aggregated at subbasins scale and routed downstream.

As shown in Figure 1a, for each HRU, there are several storage compartments, representing canopy, snowpack, soil profile (0-2 m), shallow aquifer (2-20 m), and deep aquifer (>20 m), respectively (Arnold et al., 2000; Narula and Gosain, 2013). Both the whole HRU and individual compartments are based on water balance equations. For HRU, it can be expressed by $\Delta S = P - \sum Q - \sum E$, where ΔS is the change of water storage volume within the whole HRU; P represents the precipitation, including rainfall and snowfall; Q is the water yield from different water components, including surface runoff, lateral runoff, and groundwater; E are the evapotranspiration from different parts. Snowfall might be held in the snow cover, which might melt when reaching a certain temperature threshold and become surface runoff. A part of the rainfall is retained by vegetation which later evaporates, while the rest reaches the soil surface, contributing to surface runoff or infiltration along the soil profile. There are several different pathways for soil water. It may leave by evaporation or plant uptake, laterally flow into the stream, or percolate into aquifers. Water in the shallow aquifer will eventually flow into rivers or deep aquifers. Evapotranspiration occurs in snow cover, vegetation, soil, and shallow aquifer storage, corresponding to sublimation, transpiration, evaporation, and re-evaporation.

For the soil profile, the water balance can be expressed as (Neitsch et al., 2011):

$$\Delta SW = R - E_{surf} - Q_{surf} - Q_{lat} - \omega_{seep} \tag{1}$$

where R is the precipitation reaching the soil surface; E_{surf} is the evaporation from the soil surface; Q_{surf} and Q_{lat} represent the generated surface runoff and lateral runoff, respectively; and ω_{seep} is the water flux of percolation from the soil bottom.

SWAT simulates the fate and transport of nitrogen in the soil profile and the shallow aquifer (Figure 1b). The inputs of nitrogen can be from the initial nitrogen level, fertilizer application, residues, and atmospheric deposition. There are five nitrogen (N) pools in the soil, i.e., inorganic nitrogen (NH_4^+ and NO_3^-), and organic nitrogen (fresh organic nitrogen, stable organic nitrogen, and active organic nitrogen). The transformation between different N pools occurs in the soil profile. Nitrate comes from the inputs, transformation from mineralization of organic nitrogen and nitrification of ammonia nitrogen. Furthermore, nitrate sinks can be plant uptake, denitrification, and seepage to the aquifer. Nitrate is transported between storages with water flow and released to the river based on the average concentration of the storage.

For example, water and nitrate leaching from the soil bottom recharge to the aquifer according to Eq. 10 and 11, respectively. And the nitrate load released with the groundwater is calculated by Eq. 12.

$$Q_{rchrg,i} = \left(1 - \exp\left[\frac{-1}{\delta_{gw}}\right]\right) \cdot \omega_{perc} + \exp\left[\frac{-1}{\delta_{gw}}\right] \cdot Q_{rchrg,i-1} \tag{2}$$

$$NO3_{rchrg,i} = \left(1 - \exp\left[\frac{-1}{\delta_{gw}}\right]\right) \cdot NO3_{perc} + \exp\left[\frac{-1}{\delta_{gw}}\right] \cdot NO3_{rchrg,i-1} \tag{3}$$

where $Q_{rchrg,i}$ [L] and $NO3_{rchrg,i}$ [ML^{-2}] are the amount of water and nitrate recharging to the aquifers on day i, $Q_{rchrg,i-1}$ [L] and $NO3_{rchrg,i-1}$ [ML^{-2}] are the amount of water and nitrate recharging to the aquifers on the previous day i-1, ω_{perc} [L] and $NO3_{perc}$ [ML^{-2}] are the amount of water and nitrate leaching from the soil bottom, and δ_{gw} [T] is the delay time.

$$NO3_{gw} = \frac{NO3_{sh,i-1} + NO3_{rchrg,i}}{aq_{sh,i} + Q_{gw} + \omega_{revap} + \omega_{rchrg,dp}} \cdot Q_{gw} \tag{4}$$

where $NO3_{gw}$ [ML^{-2}] is the amount of nitrate load in groundwater flow, $NO3_{sh,i-1}$ [ML^{-2}] is the amount of nitrate in the shallow aquifer at the end of day i-1, $aq_{sh,i}$ is the amount of water stored in the shallow aquifer at the end of day i, Q_{gw} [L] is the groundwater flow into the stream on day i, ω_{revap} [L] and $\omega_{rchrg,dp}$ [L] are water deficiencies moving into the soil and deep aquifer, respectively.

In Eq. 2 and 3, although the lag coefficient δ_{gw} is used to represent the lag response between input and output, the same structure of the formulas suggests that the two variables vary simultaneously, implying that both flow and nitrate are transmitted at the same rate, which is inconsistent with the "old water paradox" mentioned earlier. In addition, the constant δ_{gw} indicates that there is only one recharge path from the soil bottom to the aquifers. It is clear from Eq. 4 that the nitrate release from the shallow aquifer is based on the well-mixed assumption. The fractional part represents the average nitrate concentration in the shallow aquifer, with the numerator $(NO3_{sh,i-1} + NO3_{rchrg,i})$ and denominator $(aq_{sh,i} + Q_{gw} + \omega_{revap} + \omega_{rchrg,dp})$ representing the total amount of nitrate and stored water in shallow aquifer on day i. The assumption suggests that the water parcels from each period contribute to the outflow in volume proportions and a change of input can quickly trigger the response of the outflow concentration. Hence, the original model only reflects pressure propagation but not mass transfer. However, previous studies have demonstrated that the system could have an affinity to remove water of certain ages for outflow, related to the activation of flow paths under different ecohydrological conditions (Benettin et al., 2017; Nguyen et al., 2021; Rodriguez and Klaus, 2019; Aaron A. Smith et al., 2018; J. Yang et al., 2018). It is the limitation of SWAT in representing the internal solute transport processes, as well as the fact of many traditional hydrological models (Hrachowitz et al., 2016). Evaluating the model based on model performance is not sufficient as the model could give "right results for the wrong reasons" (Kirchner, 2006). We propose a coupled model (SWAT-SAS) to replace the original two-layer aquifer with a transport model to better represent the subsurface nitrate transport process. In the following part, we will introduce the transport model we use (SAS) and its implication for representing the diverse transport scheme, and then describe the coupling of the model.

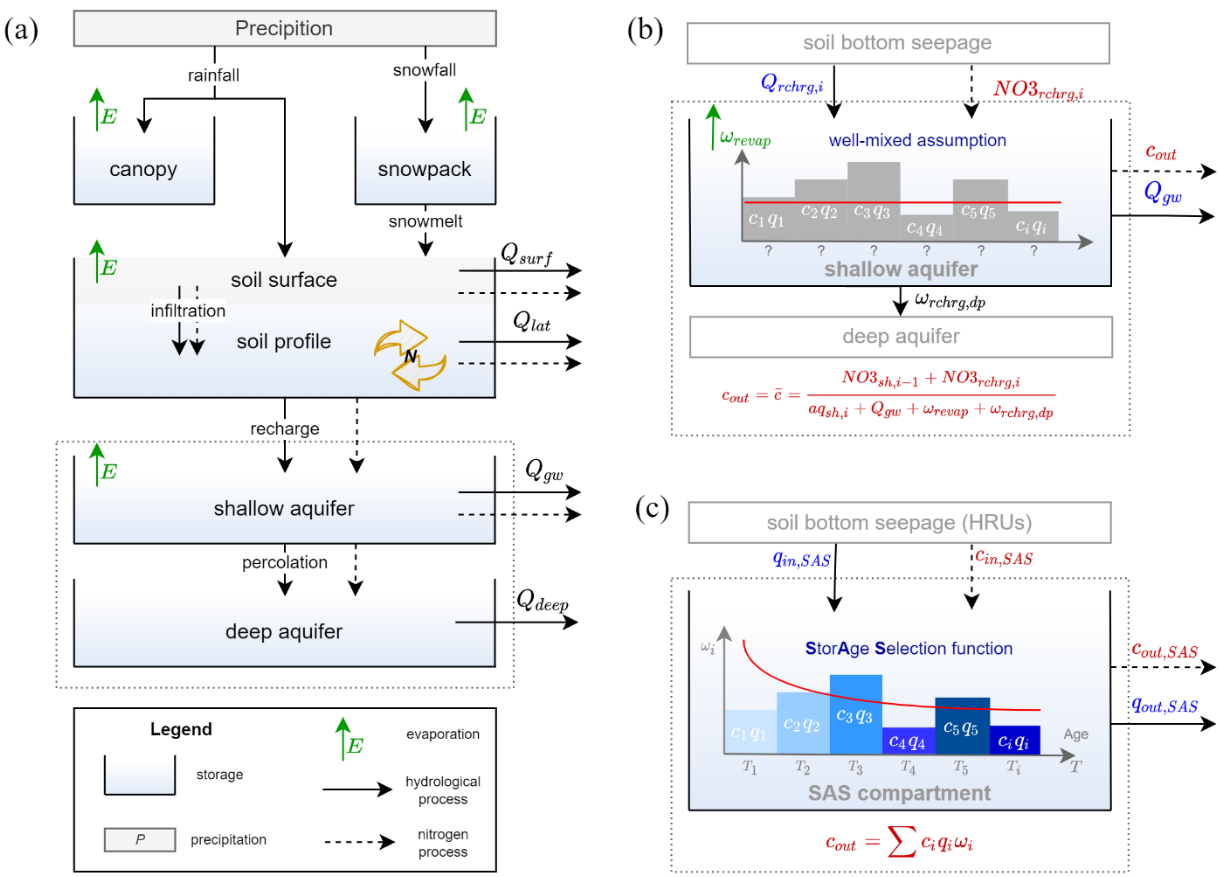

Figure 1. Schematics of SWAT model processes and SAS module. (a) Hydrological process of each HRU; (b) Nitrate transport in the aquifers of original SWAT model; (c) Replaced nitrate transport for aquifers, the SAS compartment.

2.2 The TTD model, SAS

The storage variation of the SAS compartment at any time step t can be represented by Eq. 5:

$$\frac{\mathrm{d}S}{\mathrm{d}t} = J(t) - Q(t) \tag{5}$$

where $J(t)$ [LT^{-1}] represents the seepage through the soil bottom into the aquifer at time t, and $Q(t)$ [LT^{-1}] represents the water outputs of the system at time t. Outflows and evaporation are the two major outputs for a hydrological system. In this paper, we neglect evaporation and only consider groundwater as the outflow of the system. There is a detailed description for the complete equation including discharge and evaporation in Harman's paper (2015).

The TTD can be expressed by either forward or backward form. The forward TTD denotes the destination of injected water parcels, often used to fit the breakthrough curve of tracer input. The backward TTD describes the water age distribution at the outlet and implies the contribution of different past events to the discharge. It is more suitable to use the backward form when we generally have gauge observations and want to assess the water contribution of inputs over time (Benettin P. et al., 2015; P. Benettin et al., 2015; Rinaldo et al., 2015). For SAS function applications, the backward TTD is used to quantify how catchments store and release water and solutes (Rinaldo et al., 2015; Rodriguez et al., 2021). The time that a water parcel retains in the system is defined as residence time (RT), denoted by age *T*. And the age of the water parcel leaves the system is the transit time. Based on the conservation of mass and water age, Eq.5 can be expressed as follows, indicating the change of storage with age younger than *T* depends on inflow, outflow, and storage aging (Botter et al., 2011; Harman, 2015; Velde et al., 2012).

$$\frac{\partial S(T,t)}{\partial t} = J(T,t) - Q(T,t) - \frac{\partial S(T,t)}{\partial T} \tag{6}$$

At any time, the storage of SAS compartment $S(t)$ is composed of water parcels with various ages. The fractions of the storage with different age T are characterized by a probability density distribution $p_s(T,t)$ [T^{-1}]. And the corresponding cumulative density distribution is $P_S(T,t) = \int_0^T p_S(\tau,t)d\tau$ [-], meaning the fraction of storage with age younger than *T*. At any time, the storage comprised of the past influxes and the storage with age younger than *T* can be defined as $S(T,t) = S(t)P_S(T,t)$ [L]. Similarly, the age distribution of outflux can be defined as a cumulative version, $P_S(T,t)$, and the outflux consisting of water age younger than *T* is $Q(T,t) = Q(t)P_Q(T,t)$ [LT^{-1}].

The age of water is zero when entering the system, with initial condition $S(T, t = 0) = S_{T_0}$ and boundary condition $S(T = 0, t) = 0$. Typically, the age distributions of outflow are unknown and insufficient to solve Eq. 6. The SAS function Ω_Q is introduced (Botter et al., 2011; Harman, 2015; Velde et al., 2012) and defined as the relationship between the age distribution of the storage and that of the outflux, i.e., $P_Q(T, t) = \Omega_Q(S(T, t), t)$ [-]. Then Eq. 6 can be expressed as:

$$\frac{\partial S(T,t)}{\partial t} = J(t) - Q(t)\Omega_Q(S(T,t),t) - \frac{\partial S(T,t)}{\partial T} \tag{7}$$

The cumulative and probability forms of the TTD can be converted to each other as follows:

$$p_Q(T,t) = \frac{\partial P_Q(T,t)}{\partial T} = \frac{\partial \Omega_Q(S(T,t),t)}{\partial S(T,t)} \cdot \frac{\partial S(T,t)}{\partial T} = \omega_Q \cdot \frac{\partial S(T,t)}{\partial T} \tag{8}$$

The SAS provides a mathematical expression reflecting the release preference. The formalization can be parameterized by Beta distributions (Eq. 9).

$$\omega(P_s, t) = Beta(P_s, a, b) \tag{9}$$

where a [-] and b [-] are parameters for Beta distribution. Compared to the well-mixed scheme, the SAS function is a more general framework, characterizing various preferences with different values. If $a = b = 1$, there is no preference for water age, which corresponds to well-mixed scheme; if $a > b$, there is a preference for releasing old water; if $a < b$, there is a preference for releasing young water. See reference (Harman, 2015) for more SAS function distributions and preferences schemes.

Similarly, the solute concentration of outflow is calculated by Eq. 10 (Queloz et al., 2015):

$$c_Q(t) = \int_0^\infty c_J(t-T,t) \cdot p_Q(T,t) \cdot \exp(-kT)\, dT \tag{10}$$

where $c_J(t-T,t)$ [ML^{-2}] is the solute concentration of influx at time $t-T$, and k [-] is the denitrification rate.

The residence time (RT) is distinct from the TT and refers to the time that a water parcel retains in the storage. The residence time distribution (RTD) indicates the age distribution for the water parcels in the storage. It is obvious that the RT and TT reflect the water age in storage and outflow, respectively. Mean and median values of water ages of the storage and the outflow can be further derived to characterize their age structure, i.e., *MTT*, *MRT*, TT_{50} and RT_{50}. The mean transit time of discharge, $MTT(t)$ [T], is calculated by given $p_Q(T,t)$.

$$MTT(t) = \int_0^\infty T \cdot p_Q(T,t)dT \tag{11}$$

The calculation of mean residence time (*MRT*, [T]) is calculated as follows:

$$MRT(t) = \int_0^\infty T \cdot p_S(T,t)dT \tag{12}$$

The median transit time (TT_{50}, [T]) and median residence time (RT_{50}, [T]) indicate the cumulative fraction of age-ranked water reaching 50% in discharge and storage, respectively.

2.3 SWAT-SAS: couple SAS compartment with SWAT

In SWAT-SAS, the original two-layer aquifer is conceptual as the SAS compartment (Fig. 1c) and the nitrate concentration of the groundwater is calculated by SAS algorithms. The SAS module aggregates the soil bottom seepage from different HRUs and then calculates the nitrate output at the subbasin scale, i.e., the nitrate contribution from aquifers to the stream. The time step for discretization computations and water age is days, corresponding to SWAT. Forward Euler scheme was implemented to solve the age master equation referring to *trans*-SAS (Benettin and Bertuzzo, 2018). Five parameters related to the SAS compartment were introduced. The initial conditions are initial groundwater storage (S_0, [L]) and the initial nitrate concentration (c_0, [ML-3]), which are used at the beginning of the calculations. There are two parameters for the Beta SAS function, i.e., k_a [-] and b [-], by which the shape of the Beta distribution can be adjusted. The parameter half_life [-] corresponds to the subsurface denitrification coefficient of Eq. 9. When lacking the initial information, the initial conditions can be seen as a single old pool. With the calculation, new water parcels are introduced and account for increasing proportions, hence reducing the effects of initial conditions (Benettin and Bertuzzo, 2018). Our simulation found that the initial nitrate concentration (c_0) had little effect on the results, so we calibrated the other four newly introduced parameters.

The SWAT-SAS is modified based on SWAT 2012 version 681; the modified code is compiled by Visual Studio 2019. Detailed code and compiler configuration are available on the GitHub page (https://github.com/li3uhua/SWAT-rev681).

3 Model setup

3.1 Study area and data

The study area is the Upper Selke, situated in northeast Harz Mountain, central Germany (Figure 2a). A gauging station (Silberhutte) is located at the outlet, covering a catchment area of 100.6 km^2 (Figure 2b). The catchment is an upland area with elevation ranges from 333 to 607 m and an average slope of 10.6 (Figure 2b and 2e). Forest and agricultural land are the dominant land uses, accounting for 60.2% and 19.6 % of the catchment area, respectively (Figure 2c). The soil types are quite uniform in the Upper Selke, mainly covered with Dystric Camisol (CMd) (Figure 2d).

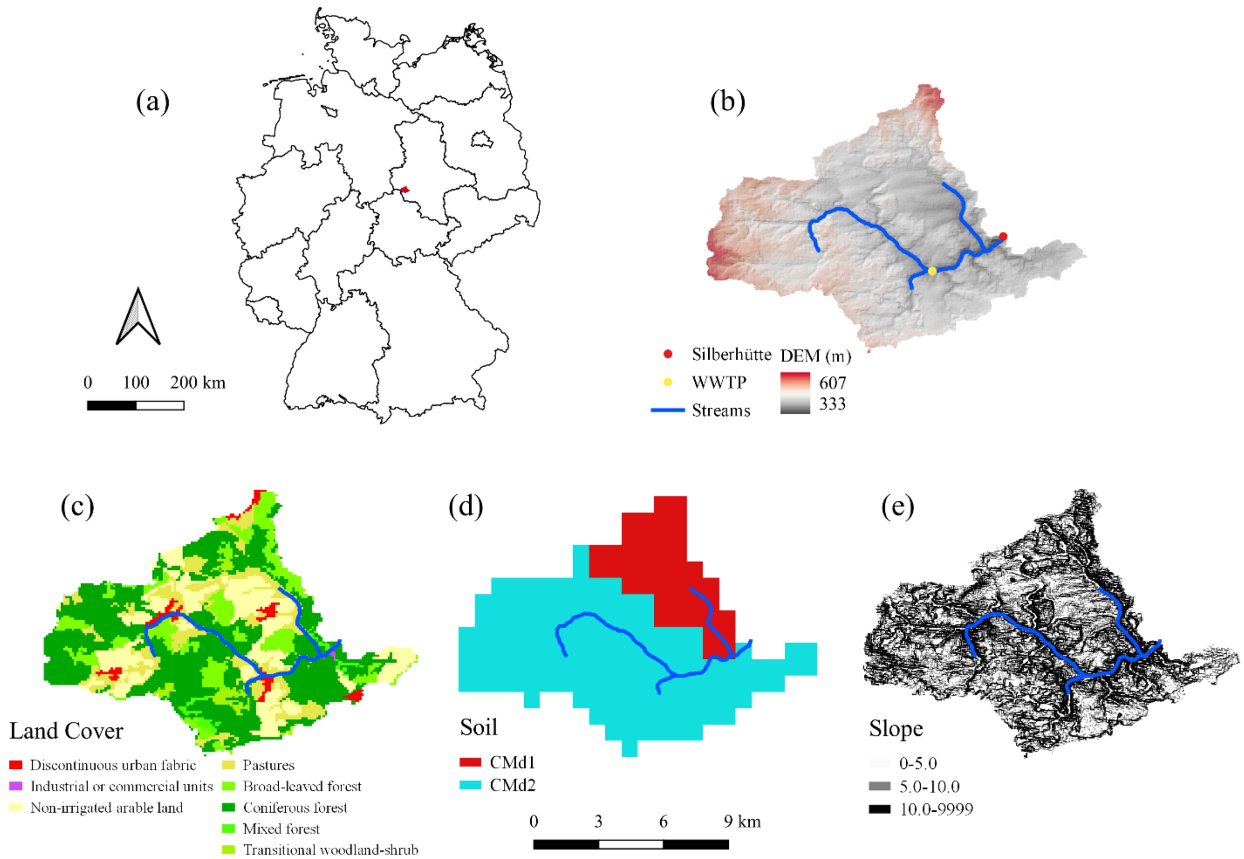

Figure 2. Spatial distribution of Upper Selke. (a) location; (b) digital elevation model (DEM), the blue lines are the streams created by SWAT; (c) land cover distributions; (d) soil class distribution; (e) slope classification.

Spatial data (including topography, land use and soil distribution), observed data (including climate, streamflow, and in-stream nitrate concentration) and survey data (such as agricultural management and wastewater treatment plants) are required for constructing a SWAT model.

The spatial data are used for watershed discretization and model parameterization, collected through different sources. A digital elevation model (DEM) with a resolution of 30 m was obtained from the SRTM website. Corine Land Cover product of 2012 (CLC2012) with 100 m resolution was obtained from Copernicus Global Land service. Soil map and characteristics were from FAO Harmonized world soil database (HWSD) v1.2. Some soil characteristics need to be calculated based on HWSD through pedo transfer functions (Abbaspour et al., 2019). The detailed calculation we used can be seen from Supplementary Material S1.

Climatic inputs provide moisture and energy to drive all processes of the model. Daily precipitation, temperature, and humidity data for 2007-2019 were obtained from the German Weather Service (DWD). There is a significant lack of wind speed and solar radiation data. These values are simulated using CFSR global weather generator data from the SWAT official website. Daily streamflow and in-stream nitrate concentrations were obtained from the State Agency for Flood Protection and Water Management of Saxony-Anhalt (LHW) and Helmholtz Center for Environmental Research (UFZ), respectively. According to the historical observations (2012-2019), the mean annual precipitation is 711 mm, and the mean annual streamflow is 0.715 m^3/s (i.e., 224 mm). The wet season of the catchment is from January to March with the an average flow of 1.62 m^3/s. July to September is the dry season with average flow of 0.30 m^3/s. Agricultural management including fertilizer application and crop rotation, was taken from the work of Yang et al. (Yang et al., 2022).

3.2 Model configuration

QSWAT3 was used to set up models, which is a visual interface in QGIS 3.16 that allows users to sequentially execute procedures for geospatial data processing and analysis, as well as editing input data.

To capture all the spatial heterogeneity, we set the thresholds for slope, soil, and land use to 0, 0, and 0, respectively, and finally get 24 HRUs. For hydrological calculation, the Hargreaves method was used to calculate potential evaporation (PET) and the SCS curve number method was used to calculate surface runoff. For nitrate simulation, we applied agricultural management and initial residues according to the survey data from the work of Yang et al. (2022). Winter wheat and rapeseed are the major crops planted in the catchment. We split the arable land into two types according to the areal share and set different managements respectively (see Supplementary Material S2 for detailed management setup). There are two wastewater treatment plants (WWTP) located in the catchment. Daily output flow and nitrate concentration were input to simulate the point source pollution.

3.3 Model calibration

After constructing the model, models were run and calibrated by R-SWAT, an interactive web-based application for parallel running, parameter sensitivity, calibration, and uncertainty analysis with SWAT (Nguyen et al., 2022a). We simulate daily runoff and nitrate concentration over the period 2007 to 2019, with five years (2007-2011) for warming up, four years (2012 to 2015) for calibration and four years (2016 to 2019) for validation. For the characteristics of transit time, the related values (MTT, TT_{50}, etc.) will keep increasing in the at beginning of the simulation period, and a more extended warming-up period is needed to reflect transit time variation. After getting the behavioral parameter sets, we ran the model for 58 years to get the transit time outputs.

SWAT is a comprehensive model with a large number of parameters, and each parameter may affect the interaction process it represents (Arnold et al., 2012). Sensitivity analysis and auto-calibration helps modelers identify the crucial parameters, improve the model performance and get the behavioral ranges efficiently (Liu et al., 2016). The sequential uncertainty fitting algorithm (SUFI-2) was used for auto-calibration. SUFI-2 performs Latin hypercube sampling of selected parameters, runs simulations based on composed parameter sets, and performs uncertainty analysis (Abbaspour et al., 2004a). The description and ranges of calibrated parameters are shown in Table 1, and the sensitivity ranking can be found in Supplementary Material S3. We first calibrated the water quantity, fitting the streamflow data to obtain the behavioral ranges of hydrological parameters, and then further calibrated the water quality parameters related to nitrogen simulation.

The performance of models was evaluated by traditional indices that are widely used for evaluating hydrological models, i.e., Nash-Sutcliffe efficiency (*NSE*) (Nash and Sutcliffe, 1970), percentage of bias (*PBIAS*) and correlation (R^2).

$$NSE = 1 - \frac{\sum\left(Q_i^{sim} - Q_i^{obs}\right)^2}{\sum\left(Q_i^{sim} - \overline{Q^{obs}}\right)^2} \tag{13}$$

$$PBIAS = \frac{\sum\left(Q_i^{sim} - Q_i^{obs}\right)}{\sum Q_i^{obs}} \times 100\% \tag{14}$$

$$R^2 = \frac{\sum\left[\left(Q_i^{obs} - \overline{Q^{obs}}\right)\left(Q_i^{sim} - \overline{Q^{sim}}\right)\right]^2}{\sum\left(Q_i^{obs} - \overline{Q^{obs}}\right)^2\left(Q_i^{sim} - \overline{Q^{sim}}\right)^2} \tag{15}$$

where Q_i^{obs} $(i = 1, 2, \ldots)$ is the series of observed daily streamflow, Q_i^{sim} $(i = 1, 2, \ldots)$ is the series of simulated daily streamflow, $\overline{Q^{obs}}$ is the mean value for the observed daily streamflow. For nitrate concentration, the performance metrics are calculated with the same formula.

Kling-Gupta efficiency (*KGE*) addresses several shortcomings of traditional indices like *NSE*, combining model errors (correlation, ratio of variances and bias) in a more balanced way (Gupta et al., 2009; Liu, 2020) . It has increasingly been used in to evaluate model performance more comprehensively (Knoben et al., 2019). The calculation of the *KGE* value is as follows:

$$KGE = 1 - \sqrt{(r-1)^2 + (\alpha-1)^2 + (\beta-1)^2} \tag{16}$$

Where r is the linear coefficient between the observed and simulated series; $\alpha = \frac{\sigma_{sim}}{\sigma_{obs}}$ is a measure of the variability error, and $\beta = \frac{\mu_{sim}}{\mu_{obs}}$, is a bias term. In our study, *KGE* is the objective function for calibration, and *NSE*, *PBIAS*, and R^2 are also calculated to refer to the criteria recommended by Moriasi (Moriasi et al., 2015, 2007).

The uncertainty of the model is measured by *p*-factor and *r*-factor. The *p*-factor is the percentage of observed data covered by the 95PPU band, ranging from 0 to 1. The model with *p*-factor = 1 means that all uncertainties are considered in the model. The *r*-factor is the average width of the 95PPU band, and the *r*-factor = 0 means the simulated series fits well with the observed data. The two factors are closely related to each other, which indicates a larger *p*-factor can be achieved at the expense of higher *r*-factor (Abbaspour et al., 2004b; Arnold et al., 2012).

Table 1. Selected parameters and calibration range.

Parameter	Description	Initial range	Final range	Optimal value
snowmelt				
SMTMP.bsn	Snowmelt base temperature (℃)	[-2, 2]	[-2, 0]	-1.92
SFTMP.bsn	Snowfall base temperature (℃)	[-2, 2]	[0, 2]	0.38
TIMP.bsn	Snowpack temperature lag factor (-)	[0, 1]	[0, 0.6]	0.50
evaporation				
ESCO.hru	Soil water evaporation compensation factor (-)	[0, 1]	[0.7, 1]	0.86
CANMX.hru	Maximum canopy storage (mm H2O)	[0, 20]	[5, 16]	13.03
water generation and regression				
CN2.mgt*	Curve number II (-)	[-0.3, 0.3]	[-0.05, 0.1]	0.04
SOL_K.sol*	Saturated hydraulic conductivity of soil layer (mm/hr)	[-0.2, 0.2]	[-0.2, 0.2]	0.18
SOL_AWC.sol*	Available water capacity of soil layer (mm H2O/mm soil)	[-0.2, 0.2]	[-0.15, 0.15]	0.09
GWQMN.gw	The threshold depth of water in the shallow aquifer required for return flow to occur (mm)	[0, 2000]	[0, 1000]	494.03
RCHRG_DP.gw	Deep aquifer percolation fraction (-)	[0, 0.3]	[0, 0.3]	0.27
SURLAG.hru	Surface runoff lag time (day)	[0.05, 5]	[0.05, 0.2]	0.11
LAT_TTIME.hru	Lateral flow travel time (day)	[0, 30]	[0, 25]	18.10

Parameter	Description	Initial range	Final range	Optimal value
GW_DELAY.gw	Groundwater delay (day)	[0, 300]	[5, 20]	11.67
ALPHA_BF.gw	Base flow recession constant (1/day)	[0, 1]	[0.5, 1]	0.74
channel routing				
CH_K2.rte	Effective hydraulic conductivity (mm/hr)	[0, 10]	[2, 10]	2.61
CH_N2.rte	Manning's "n" value for the main channel (s m-033)	[0, 0.1]	[0.004, 0.08]	0.05
nitrogen simulation				
SHALLST_N.gw	The concentration of nitrate in groundwater contributes to streamflow from subbasin (mg N/L)	[0, 100]	[0, 100]	98.89
RCN.bsn	Concentration of nitrogen in rainfall (mg N/L)	[0, 15]	[0, 6]	2.34
ERORGN.hru	Organic N enrichment ratio (-)	[0, 1]	[0.5, 1]	0.58
SOL_CBN.sol	percent organic carbon in soil layer (%)	[0, 10]	[5, 10]	13.65
CDN.bsn	Denitrification exponential rate coefficient (-)	[0, 1]	[0, 0.1]	0.002
NPERCO.bsn	nitrate percolation coefficient (0-1)	[0, 1]	[0, 0.2]	0.03
N_UPDIS.bsn	Nitrogen uptake distribution parameter	[0, 100]	[10, 80]	33.80
RSDCO.bsn	Residue decomposition coefficient (-)	[0, 1]	[0.2, 0.7]	0.80
SDNCO.bsn	Denitrification threshold water content (-)	[0, 1]	[0.5, 1]	0.99
ANION_EXCL.sol	Fraction of porosity (void space) from which anions are excluded (-)	[0, 1]	[0.5, 0.8]	0.79
HLIFE_NGW.gw	Half-life of nitrate in the shallow aquifer (days)	[0, 300]	[100, 260]	212.01
SOL_NO3.chm	Initial NO3 concentration in the soil layer (mg N/L)	[0, 100]	[50, 100]	76.87
SAS parameters				
S0.sas_param.par	Initial groundwater storage (mm)	[0, 2000]	[1000, 1800]	1792.82
ka.sas_param.par	parameter of the beta(ka,b) function (-)	[0.05, 1]	[0.6, 0.8]	0.73
b.sas_param.par	parameter of the beta(ka,b) function (-)	[0.05, 10]	[4, 5]	4.08
half_life.sas_param.par	Subsurface denitrification (1/day)	[0.01, 0.1]	[0.01, 0.06]	0.03

Note: Parameters are adjusted mainly by the replace method, except for the parameters marked with *, which are adjusted by the relative value method.

4 Results and discussion

4.1 Model performance

The performance of the models is shown in Table 2. The evaluation indices indicate that streamflow hydrographs were well reproduced by SWAT. The overall performance of daily streamflow is *KGE* = 0.78, *NSE* = 0.62, *PBIAS* = -7.2 % and R^2 = 0.64. Considering the three traditional indices, *NSE*, *PBIAS*, and R^2, the simulated results reach the criteria of “Satisfactory” according to the recommendations of Moriasi et al. (2015). In addition, a high *KGE* value also reflects good correspondence between the simulated and observed discharge.

Generally, the calibration period has better model performance than the validation period. However, the indices for the validation period outperformed those for the calibration period in our runoff simulation. This is because in all cases, there is no ideal optimization routine to find the parameter set that gives the highest possible model performance, or ideal model concept/structure that works equally well for all the periods (calibration/validation) given the uncertainty and unbiased datasets among different time-periods (Arsenault et al., 2018; L. Chen et al., 2022). Only the behavioral model performance can be achieved for the calibration period, considering uncertainty in the observed data. That is, a model that fits the calibration data better may not always necessarily better, as there may be errors in the calibration data. There could be an uncertain process in the calibration period that has not been fully accounted for, making the model cannot calibration data better than the validation data. The unusual results in our study may be attributed to the catchment experiencing a severe and long drought in 2018-2019 (Rakovec et al., 2022), and the anomalous hydro-metrological conditions could result in either better or worse performance (Nangia et al., 2008; Nguyen et al., 2022b, 2020).

Water quality simulation involves more complexity and uncertainty than water flow (Ejigu, 2021). In addition to the uncertainty of the input data and parameters, the performance of nitrate concentration is also related to the uncertainty of the simulated streamflow, and hence is relatively poor compared to the streamflow. The indices for the original SWAT daily nitrate simulation are *KGE* = 0.68, *NSE* = 0.38, *PBIAS* = -3 % and R^2 = 0.46, while the indices for SWAT-SAS are higher with *KGE* = 0.78, *NSE* = 0.55, *PBIAS* = 3.7 % and R^2 = 0.62. The performance of SWAT-SAS is generally better than SWAT, partly due to the additional SAS parameters providing more freedom and flexibility to the simulation, and partly due to the simplification of nutrient transport processes by SWAT. Comparing the *p*-factors and *r*-factors for the simulation period, the *p*-value for SWAT-SAS (*p*-factor = 0.63) is higher than SWAT (*p*-factor = 0.49). However, its *r*-factor (*r*-factor = 0.97) increased relative to SWAT (*r*-factor = 0.78).

Table 2. Performance of streamflow and nitrate concentration simulations

Period	Streamflow				Nitrate concentration (SWAT)				Nitrate concentration (SWAT-SAS)			
	KGE	*NSE*	*PBIAS*	R^2	*KGE*	*NSE*	*PBIAS*	R^2	*KGE*	*NSE*	*PBIAS*	R^2
Daily												
Calibration	**0.71**	0.57	-10.9	0.59	**0.66**	0.29	9.6	0.47	**0.67**	0.4	15.8	0.61
Validation	**0.84**	0.69	-2.7	0.72	**0.64**	0.44	-15.5	0.5	**0.79**	0.66	-8.2	0.67
Overall	**0.78**	0.62	-7.2	0.64	**0.68**	0.38	-3	0.46	**0.78**	0.55	3.7	0.62
Weekly												
Calibration	**0.76**	0.64	-10.9	0.66	**0.68**	0.33	9.2	0.49	**0.68**	0.43	15.3	0.63
Validation	**0.86**	0.74	-2.9	0.78	**0.64**	0.45	-15.7	0.51	**0.79**	0.67	-8.6	0.68
Overall	**0.83**	0.69	-7.2	0.71	**0.69**	0.4	-3.5	0.48	**0.79**	0.57	3.1	0.63
Monthly												
Calibration	**0.82**	0.69	-10.9	0.73	**0.78**	0.57	8.4	0.66	**0.69**	0.5	15	0.7
Validation	**0.9**	0.87	-2.7	0.89	**0.65**	0.47	-16.3	0.53	**0.79**	0.68	-9	0.7
Overall	**0.87**	0.79	-7.2	0.81	**0.74**	0.51	-4.5	0.56	**0.81**	0.61	2.4	0.67

4.2 Simulated streamflow and nitrate concentration

The series and the exceedance probability curves of the simulated results are shown in Figure 3, which visually illustrates the coincidence of the observed and simulated values.

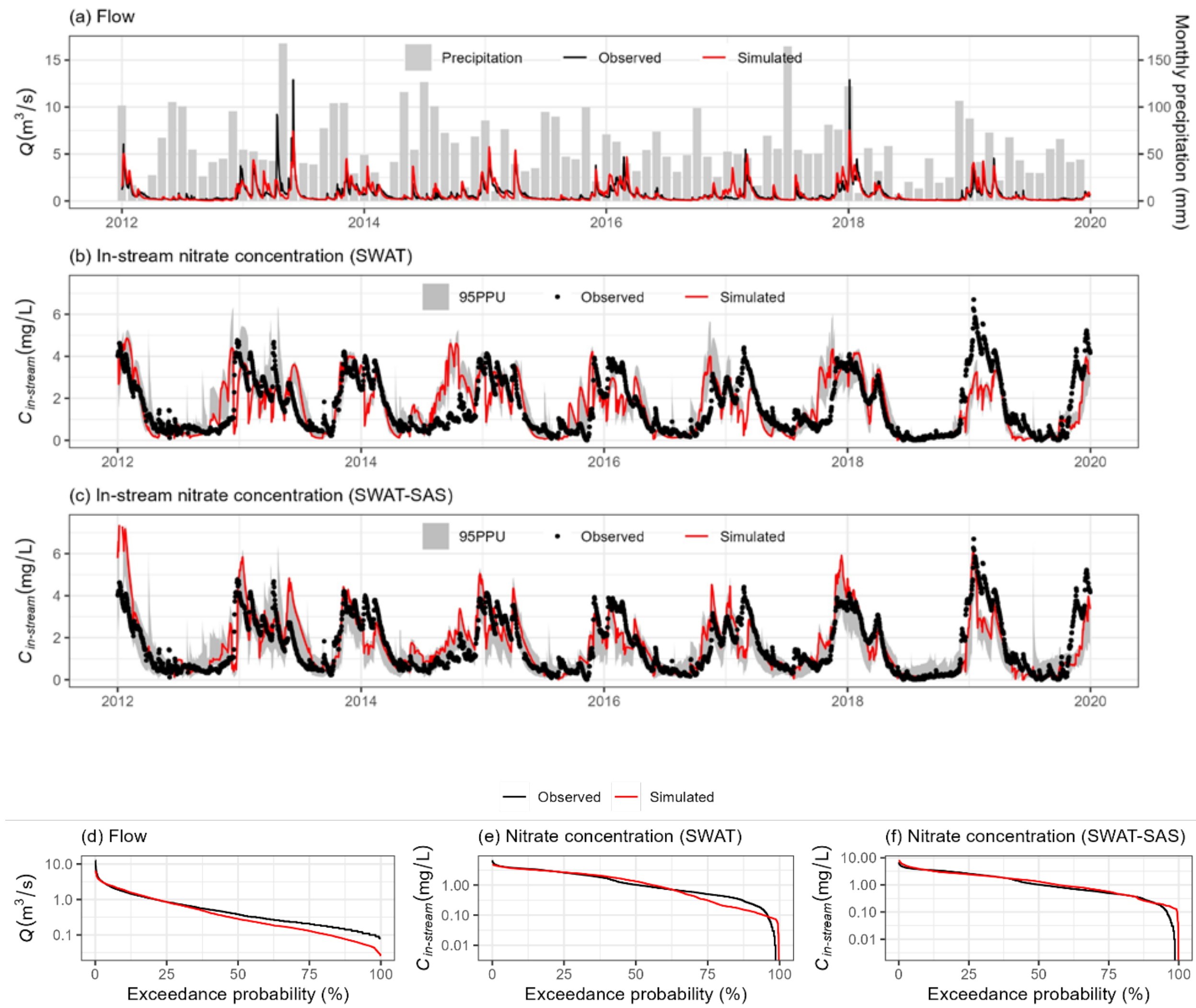

Figure 3. Series and exceedance probability curves for observed and simulated data.

As shown in Figure 3a, the hydrographs were well reproduced, and the simulated results intuitively fit well with the observed series. However, the models did not simulate low flows properly even after a comprehensive calibration, and the underestimations become more pronounced at lower flows, which can be seen from the exceedance probability curve (Figure 3d). There may be two reasons for the poor performance in the dry season. One is that the flow in the wet season contributes more to the objective functions (Zhang et al., 2015), and the other is the limitation of the groundwater module (Kim et al., 2008). Almost all observed flow peaks were captured, but incorrect peaks were predicted around January. It might be related to the limitation of the snow module that restricts water infiltration and generates more surface runoff during snow events (Qi et al., 2016). These limitations are not the subjects of this study and cannot be overcome by our modified model. We point out these estimation errors to analyze the nitrate simulation results more comprehensively. In addition, the uncertainty in the rainfall data could also contribute to the biases of individual high discharge events, as noted by Nguyen et al. (2021).

Both original SWAT and SWAT-SAS can capture the magnitude of nitrate concentrations and reflect the seasonal variations to some extent (Figure 3b-c), showing high nitrate concentration values in wet seasons and low nitrate concentration values in dry seasons. Intuitively, SWAT-SAS better reflected the rising and falling limbs of nitrate concentrations, while the original SWAT often showed an early peak, which are also found in other studies based on distributed models (Hesser et al., 2010). For example, there was an early peaks simulated by SWAT in late 2012, 2014, and 2017. SWAT-SAS better matched to the observed values for the corresponding period, although still with an early peak.

Both models overreacted to the nitrate concentration and the temporal dynamics were not properly captured. This can be explained by the uncertainty arising from model structural issues or input data. In addition to groundwater, surface runoff and lateral flow also transport nitrates that affect the in-stream nitrate concentrations. These two components have more rapid impacts on the water quality, resulting in overreactive dynamics. According to the modeling results, the annual water yield of the catchment is 208.4 mm, of which surface runoff is 67.7 mm (32.5%), lateral flow is 15.6 mm (7.5%), groundwater from shallow aquifer is 91.2 mm (43.8%) and groundwater from deep aquifer is 33.8 mm (16.2%). And the nitrate loads discharged to the river with the transport of each component are 0.1 kg/ha, 0.46 kg/ha and 4.13 kg/ha, respectively. Previous findings have also shown that the catchment is dominate by shallow sub-surface flow, and the other water components mainly occur in wet season (Sinha et al., 2016). Although the surface runoff concentration is relatively low, the high flow rate may dilute the output concentrations rapidly. Additionally, although the lateral flow accounts for a small proportion, it scours the soil and carries relatively high nitrate concentrations, which will increase the output concentrations. The scouring and dilution effects may prevail under varying moisture and rainfall conditions, exhibiting seasonal variability (X. Zhang et al., 2020). Whereas the improvements we made to the model were limited to the nitrate transport processes of the aquifers and could not improve the effects of other runoff components. Furthermore, water quality modeling is also susceptible to the simulated streamflow, and the weaker performance of the model at low flows can also introduce errors to water quality modeling.

The nitrate exceedance probability provides an evaluation of the agreement between the simulated and observed values in statistical sense (Figure 4e-f). For high nitrate concentrations (exceedance probability < 25 %), the original SWAT generally underestimates while SWAT-SAS overestimates, such as the peaks in 2012 and 2013. For mid-level nitrate simulation (25 % < exceedance probability < 75 %), SWAT and SWAT-SAS showed good agreement with observations. For low-level nitrate simulation (exceedance probability > 75 %), SWAT deviations were significantly greater than those of SWAT-SAS. The original model may underestimate the low concentrations, resulting in incorrect assessment of water quality.

Previous studies (J. Yang et al., 2018; X. Zhang et al., 2020) defined four periods of the catchment based on streamflow and subsurface storage conditions, i.e., wetting (November to December), wet (January to April), drying (May to June) and dry (July to October) periods. We adopted the definition to further analyze the relationship of streamflow and nitrate concentration (the *C*-*Q* relationship). The *C*-*Q* relationship is plotted in log scale space, as shown in Figure 4. The positive *C*-*Q* slopes indicate the enhanced hydraulic processes are the principal mechanism driving the concentration variations (Godsey et al., 2009; Neira, 2019) and also indicates the additional activation of more shallow and younger or more distant nutrient source zones (Bowes et al., 2015; Musolff et al., 2015). In the wet season, the variation of nitrate concentration is closely related to the streamflow, and the data are uniformly distributed around the fitted line (Figure 4a). In other seasons, there are scatters far away from the fitted line. The scatters in the upper left of the fitted line indicates lower flows with higher nitrate concentration, commonly observed in the early wet season. Apart from the wet season, some scatters are distributed in the lower left of the fitted line, indicating low flows with low nitrate concentration. Other studies have noted that the low-magnitude events with low nitrate loadings occurred mainly during summer and autumn (Winter et al., 2022). It can be explained by two aspects, namely the decreased hydrological connectivity due to lower antecedent soil moisture, and the lower nitrate availability due to higher biogeochemical removal and biological uptake in summer and autumn (Musolff et al., 2015; J. Yang et al., 2018). The two models show comparable *C*-*Q* relationships, but the fitted slope of SWAT-SAS is more in line with the observed data. In addition, neither model captured outliers during the drying and dry seasons. The bias may arise from two sources, one is the simulation bias of low flow periods, and the other one is the limitation of hydrological models in dry seasons (Fowler et al., 2021; Wen et al., 2021). Since the parameters for the SAS function are invariant over the simulation range (i.e. the aquifer maintains constant age preference), the SWAT-SAS results are also biased in dry seasons.

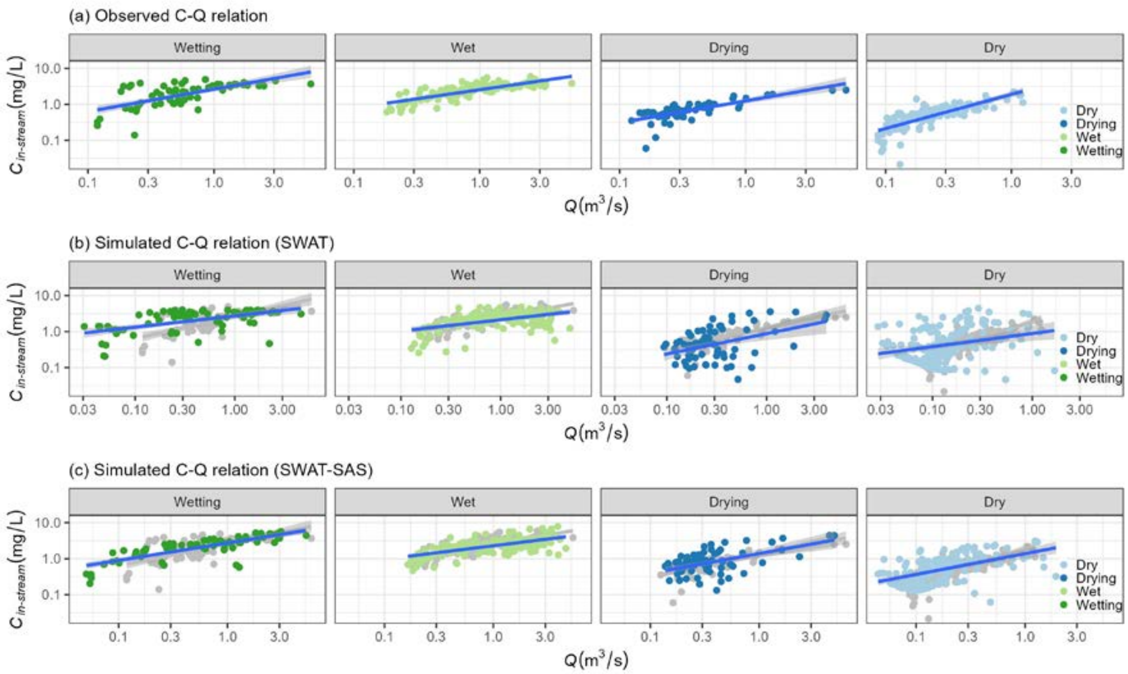

Figure 4. *C-Q* relationship in log scale. (a) observed data, (b) simulated by SWAT, (c) simulated by SWAT-SAS.

4.3 Aquifer dynamics and model comparisons

To compare the differences between SWAT and SWAT-SAS for nitrate transport within the aquifers, we conducted and analyzed two simulations. Both simulations used the same original hydrological and water quality parameters (the best parameter set for SWAT), and SWAT-SAS has five additional parameters for the SAS function. Thus, the two simulations have the same surface and soil processes and corresponding calculated results. For the aquifer system, the inputs are the same, but the output nitrate loads and concentrations are different due to the distinct nitrate transport schemes.

A large proportion of nitrate leached from the soil bottom into the aquifers, with an annual average of 45.5 kg/ha. Arable land contributed about 50% of the total leaching, while about 28% of leached nitrate came from forest land, see Supplementary Material S4 for the distribution of leached nitrate. Both models consider the transport process and decay rate in the aquifers. In SWAT, the nitrate transport is based on the well-mixed assumption at HRU scale. The model calculates the nitrate loads by using the average concentration of the shallow aquifer in each HRU, as shown in Eq.4. In SWAT-SAS, the processes of mixing and transport are aggregated into a functional form that indicates a selection scheme for different water age storage. The SAS function was parameterized with the values a = 0.73 and b = 4.08, which indicates a bias towards releasing young water (a/b < 1). Additionally, nitrate within the aquifer will decay, represented by HLIFE_NGW and half_life in SWAT and SWAT-SAS, respectively.

As shown in Figure 5a, the two simulations have comparable performance levels, with evaluation metrics for SWAT being KGE = 0.69 and for SWAT-SAS being KGE = 0.79. Notably, SWAT tends to overestimate at the start of the wet season (e.g., in late 2014, 2015, 2016 and 2017) and has a smoother change in simulated values than SWAT-SAS during the wet season. For the peak simulation of in-stream nitrate concentration ($C_{in-stream}$), it is typically observed that SWAT underestimates (e.g., January 2012 and January 2019). In contrast, SWAT-SAS tends to overestimate (e.g., January 2012, March 2013, and December 2017).

Figure 5b and 5c reflect how the two aquifer release schemes contribute to output nitrate concentration (C_{out}) and nitrate stores (ΔN_{store}). SWAT shows a fast peak in the early wet season and long tails (Figure 5b). It is because at the beginning of the wet season, the water storage of the aquifer is at a low level, higher inputs of nitrate concentration can significantly cause changes in the aquifer concentration. However, due to the increasing aquifer storage and decreasing nitrate input concentration, the impact of the nitrate input become smaller and is averaged out, resulting in more smooth changes in output concentrations during late stages. The red line in Figure 5b represents the aquifer output nitrate concentration simulated by SWAT-SAS. It shows more significant rapid concentration peaks and long tails. The peaks are sharper and sometimes are overestimated. From the fitted SAS function, young water contributes more to the outflow, and the young water normally carries higher nitrate concentration, hence the output concentration can respond quickly to the input. In Figure 5c, ΔN_{store} is calculated by the cumulative sum of daily nitrate input store and output store, reflecting the balance within the aquifers during 2012-2019. At the beginning of 2012, the nitrate store was 0, and it gradually accumulated and released with the percolation and transport processes. At the end of the dry season, the nitrate store is at a relatively low level due to the long-term lack of nitrate input and continuous decay. With the coming of the wet season, nitrate leached from the soil bottom with flow and recharged the nitrate store of the aquifers gradually. In the early wet season, the nitrate concentration inputs are relatively high, resulting in a rapid increase in nitrate store. The subsequent nitrate concentration inputs are lower, causing a certain degree of fluctuations in nitrate store. Additionally, the ΔN_{store} for SWAT-SAS usually drops to a low point within a few months, making the simulation for SWAT generally had higher ΔN_{store} than SWAT-SAS (Figure 5c). Both simulations have low $C_{in-stream}$ levels during the dry season (Figure 5a). The nitrate store simulated by SWAT-SAS is low in this period, hence making low output concentration. While for SWAT, although there is still some level of nitrate storage in the aquifer (Figure 5c), it is only stored in the shallow aquifer. While the outflow from the aquifers in dry conditions consists mainly of the deep groundwater, which does not carry nutrients or contribute to the in-stream concentration. For the wet season from late 2018 to April 2019 with arid preconditions, the SWAT-SAS was able to simulate the peak while SWAT appeared to underestimate it, indicating that the fitted SAS function can also represent the arid period to some extent.

In our study, the SAS parameters were kept constant parameters with the implication of young water preference. This scheme makes the output concentrations highly influenced by young water and is susceptible to overestimation when fertilizer and heavy rainfall coincide. For example, the high valuations in March 2013. In addition, it is less likely to apply fertilizer under conditions of intense rainfall in practical agricultural management, and therefore the errors for this period may also arise from input uncertainty. With the well-mixed assumption, this case can be averaged by the water storage and thus SWAT generates lower values. Additionally, constant SAS parameters will be questionable sometimes for some cases because the age preference might change as the conditions like storage, input force and moisture change (P. Benettin et al., 2015; Harman, 2015; Heidbüchel et al., 2019; J. Yang et al., 2018). The bench-scale hillslope experiment by Meira et al. (2022) indicated that the contribution of old water and young water varied with the wetting conditions. In 2013-2014, the catchment experienced a long-wet period. From October 2013 to March 2014, SWAT-SAS generally underestimated during the wet season while SWAT could well capture the pattern. Before the wet season, the catchment was relatively humid, with the previous wet season lasting until June. In addition, there was intense rainfall in May, with high monthly rainfall (Figure 3a). The SWAT-SAS produced high concentrations and less nitrate was stored in the aquifers. In contrast, the SWAT released nitrate slowly and until October, the ΔN_{store} remained at a relatively high level (Figure 5c). Thus, in the following wet season, the initial ΔN_{store} differed between the two simulations, making distinct output concentration levels.

For watershed management, information such as nutrient legacy also needs to be assessed to prevent excessive nutrients accumulation in the catchment and deterioration of groundwater quality. As seen from the above comparisons, although SWAT and SWAT-SAS generate similar levels of nitrate concentration outputs, the results are based on different subsurface transport models. For example, in SWAT, the rapid concentration increase in the wet season is attributed to relatively low water storage, while in SWAT-SAS, it is attributed to young water preference. And the diverse mechanisms also lead to distinct levels of nutrient legacy in the system. The scarcity of field data prevents us from determining which scheme better characterizes the nitrate legacy (Lutz et al., 2022). Despite accompanying uncertainties, SWAT-SAS enhances the flexibility to represent various schemes and helps to track different event inputs (by tagging the volumes with water age) and evaluate their long-term effect. In the next section, we will discuss the characteristics of the water age that transit time models offer, as well as the potential of water age for supporting catchment management.

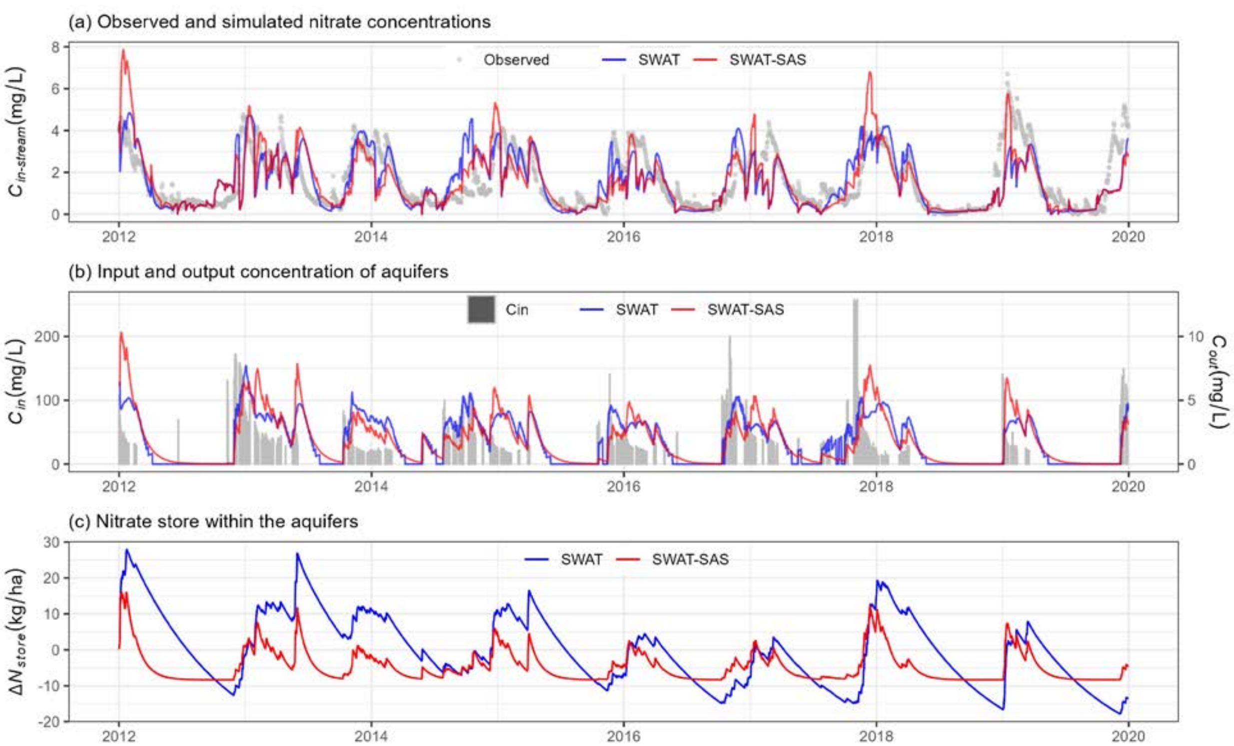

Figure 5. The performance of the two simulations and simulated aquifer. (a) simulated in-stream concentrations of the two simulations (blue line for SWAT, and red line for SWAT-SAS) compared with the observed data (grey points); (b) simulated input aquifer concentrations (grey columns) and output aquifer concentrations (blue line for SWAT, red line for SWAT-SAS); (c) nitrate store balanced within the aquifers (blue line for SWAT, red line for SWAT-SAS).

4.4 Water age characteristics of aquifers

In addition to the hydrological and water quality series, SWAT-SAS provides water age information for the control volume outflow and storage. The mean (*MTT* and *MRT*) and median (TT_{50} and RT_{50}) values of water age distribution are often used to describe the characteristics of the age structure. Figure 6 shows the variation of these indexes for the outflow and storage of the SAS compartment, with colored lines indicating the mean values of behavioral simulations, and the light color band indicating the range of these simulations.

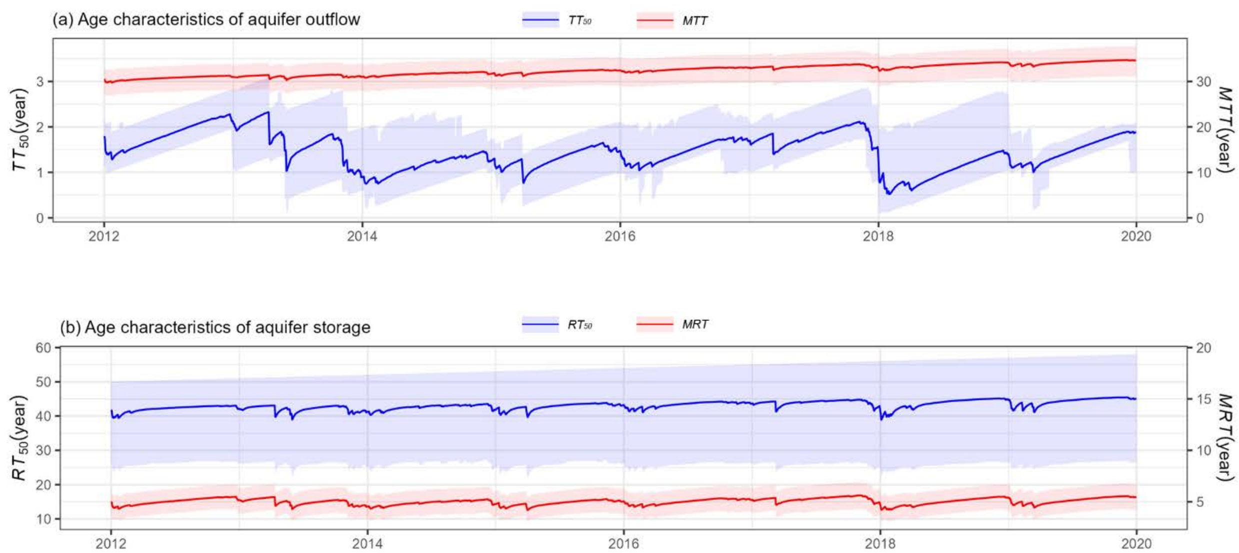

Figure 6. Characteristics of water age in discharge and storage. (a) median (TT_{50}) and mean (*MTT*) values of transit time; (b) median (RT_{50}) and mean (*MRT*) values of residence time.

The water always keeps aging, with a linear increase in age, which is evident in the dry season. The mean and median values decrease when younger water leaches and refreshes the volumes, generally occurring in the wet season. It is apparent that TT_{50} shows the greatest seasonal variation. TT_{50} represents the youngest 50% in outflow and is most affected by young water. In the wet season, sufficient young water (normally with higher nitrate concentration) constitutes a greater proportion of the outflow. The shorter transit time indicates faster transport and less time for mixing and denitrification (with less dilution and decay) during the period, explaining the rapid response and peaks of in-stream nitrate concentration noted in the previous section. Due to the lack of young water during dry seasons, the system discharges older water, resulting in a larger TT_{50}. There was a drought during 2018-2019, the TT_{50} experienced a brief decrease in a short-wet season and then increased continuously.

The other three statistical values for water age distribution (i.e., RT_{50}, *MTT* and *MRT*) are of greater values and show smaller seasonal variations. It is because they are greatly affected by the old water volume. We did not set a maximum water age to merge the old water volumes above the threshold, which allows reflecting the impact of very old water on the ages. For aquifers, the storage capacity is generally very large, and hence has long turnover time and updates slowly.

Due to the system preferring to release young water, there are large skews of the water age distribution in outflow and storage. Their median and mean values differ considerably, by about one magnitude. During the output period (2012-2019), TT_{50} ranges from 0.5 to 2.3 years, while *MTT* ranges from 29.7 to 34.7 years ($TT_{50} << MTT$), indicating that there is a long tail on the right side of the median value and the age distribution is left-skewed; RT_{50} ranges from 38.9 to 45.4 years, while *MRT* ranges from 4.2 to 5.6 years ($RT_{50} >> MRT$), indicating that there is a long tail on the left side of the median value and the age distribution is right-skewed. The statistical values also suggest that much of the water in storage is much older than the water in discharge. In storage, 50% of the water is older than 40 decades, while in discharge, 50% consists of water younger than 1.5 years.

Our modified model did not consider the transit time of soil, which is also an important field of nutrient legacy (Kumar et al., 2020). In previous work, Nguyen et al. (2022b, 2021) developed mHM-SAS and conceptualized the subsurface process as an SAS compartment, including the soil profile and aquifer system. The characteristics of water age are influenced by groundwater as well as interflow. The water age simulated by mHM-SAS was generally smaller than our results, especially in wet seasons. This is because the water age of interflow is normally younger than groundwater (Sprenger et al., 2019), and in wet seasons, contributes more to the discharge. In addition, different SAS parameters were set for the dry and wet seasons, which related to the activation and deactivation of fast shallow flow paths under variable wetness conditions. Whereas the SWAT-SAS in our study inherits the spatial variation of soil from the original model. The seasonal variations in storage selection and flow paths are not significant for the aquifers in Upper Selke, and thus the constant SAS function we used gives satisfactory results. However, for systems with more complicated aquifers, such as karst catchments, the seasonal variations of flow paths still need to be noted.

Nitrate legacy has substantial implications for assessing related measurement and management decisions, as well as environmental policies (Ascott et al., 2017; Basu et al., 2022). Neglecting the legacy issue may lead to misestimation of the timeline for achieving pollution reduction plans (Basu et al., 2022; S. Chen et al., 2022), such as the cases in the Mississippi River Basin (Meter et al., 2018), Chesapeake Bay (Chang et al., 2021; Chesapeake Progress, n.d.), Yongan watershed (Chen et al., 2017) etc. By augmenting SWAT with SAS, we can better tackle legacy issues, including when the nitrate is in and out of the system, as well as how the system is storing and releasing the nitrate. The simulated water age structure helps us to quantitively estimate the long-term effects of historical inputs on the system and more accurately simulate nitrate flux and concentrations in receiving water bodies (Basu et al., 2022; Lutz et al., 2022). For instance, if a system tends to release young water, we should be aware that the old water nitrate remains in the system and its effect on the output concentration. Despite stopping nitrate inputs, the nitrate legacy will still result in higher concentrations. A system with longer transit times can increase contact between the water and the surrounding environment, potentially resulting in higher levels of pollutants and contaminants. There are already calls for modeling studies to include, report and critically analyze model-internal N fluxes and stores in addition to output concentrations (Lutz et al., 2022).

5 Conclusions

TTD/SAS theory has been rapidly developed recently. It is becoming a robust link between hydrological and water quality processes, which is considered to compensate for the oversimplification of subsurface processes by traditional PBHMs. In our study, we reconsidered the SWAT mixing and transport processes within the aquifers and replaced the original algorithm with SAS module, calculating the aquifer nitrate concentration by SAS function. We applied the original and modified models for Upper Selke (about 100 km^2). Then, we compared the results of the models to analyze the differences between the water release schemes and discuss the potential of the modified model for supporting watershed management. The main results we come up with include:

a. The time-variant TTD model, SAS function, was successfully coupled into SWAT. It enables the modified model to represent more flexible storage release schemes of aquifers.
b. Both original (SWAT) and modified (SWAT-SAS) models can reproduce the dynamics of streamflow and in-stream nitrate concentration of the Upper Selke catchment with satisfactory performance.
c. Although the two models simulate similar levels of in-stream concentration output, the storage and concentration output within the aquifers/SAS compartment differ significantly. The differences are related to the model structure and storage selection scheme.

d. SWAT-SAS provides more information such as the age structure of the aquifer and can be used to estimate nutrient legacy for watershed management.

Although our work reconsidered the groundwater processes and provided tools for flexible representation, the determination of the transit time and nutrient legacy still requires the field data to ensure “getting the right answers for the right reasons” (Kirchner, 2006; Lutz et al., 2022; Rodriguez et al., 2021). Due to the heterogeneity of subsurface processes, the distributed application of transit time models would theoretically better represent the process variation. However, this could cause over-parameterization problems and there is still no research on how to parameterize SAS parameters at the HRU scale or the grid scale (Nguyen et al., 2021). Overcoming the over-parameterization will be a challenge for further hydrological models coupled with SAS applications. In addition, there are other methods for calculating transit time besides SAS, and comparisons between different methods are encouraged to provide a more complete analysis of the applicability and limitations of different schemes.

Competing interests: The authors declare that they have no competing interests.

Acknowledgments: This work was supported by the National Natural Science Foundation of China (52209088), Guangdong Basic and Applied Basic Research Foundation (2020A1515111152), and Guangxi Key R&D Program (AB18221108). We thank the China Scholarship Council (CSC) for providing financial support for Wuhua Li’s stay in Germany and the international academic collaboration.

References

Abbaspour, K.C., Johnson, C.A., van Genuchten, M.Th., 2004a. Estimating Uncertain Flow and Transport Parameters Using a Sequential Uncertainty Fitting Procedure. Vadose Zone J. 3, 1340–1352. https://doi.org/10.2136/vzj2004.1340

Abbaspour, K.C., Johnson, C.A., van Genuchten, M.Th., 2004b. Estimating Uncertain Flow and Transport Parameters Using a Sequential Uncertainty Fitting Procedure. Vadose Zone J. 3, 1340–1352. https://doi.org/10.2136/vzj2004.1340

Abbaspour, K.C., Vaghefi, S.A., Yang, H., Srinivasan, R., 2019. Global soil, landuse, evapotranspiration, historical and future weather databases for SWAT Applications. Sci. Data 6, 263. https://doi.org/10.1038/s41597-019-0282-4

Arnold, J.G., D. N. Moriasi, P. W. Gassman, K. C. Abbaspour, M. J. White, R. Srinivasan, C. Santhi, R. D. Harmel, A. van Griensven, M. W. Van Liew, N. Kannan, M. K. Jha, 2012. SWAT: Model Use, Calibration, and Validation. Trans. ASABE 55, 1491–1508. https://doi.org/10.13031/2013.42256

Arnold, J.G., Muttiah, R.S., Srinivasan, R., Allen, P.M., 2000. Regional estimation of base flow and groundwater recharge in the Upper Mississippi river basin. J. Hydrol. 227, 21–40. https://doi.org/10.1016/S0022-1694(99)00139-0

Arnold, J.G., Srinivasan, R., Muttiah, R.S., Williams, J.R., 1998. Large Area Hydrologic Modeling and Assessment Part I: Model Development1. J. Am. Water Resour. Assoc. 34, 73–89. https://doi.org/10.1111/j.1752-1688.1998.tb05961.x

Arsenault R., Brissette F., Martel J.-L., 2018. The hazards of split-sample validation in hydrological model calibration. J. Hydrol. 566, 346–362. https://doi.org/10.1016/j.jhydrol.2018.09.027

Ascott, M.J., Gooddy, D.C., Wang, L., Stuart, M.E., Lewis, M.A., Ward, R.S., Binley, A.M., 2017. Global patterns of nitrate storage in the vadose zone. Nat. Commun. 8, 1416. https://doi.org/10.1038/s41467-017-01321-w

Basu, N.B., Meter, K.J.V., Byrnes, D.K., Cappellen, P.V., Brouwer, R., Jacobsen, B.H., Jarsjö, J., Rudolph, D.L., Cunha, M.C., Nelson, N., Bhattacharya, R., Destouni, G., Olsen, S.B., 2022. Managing nitrogen legacies to accelerate water quality improvement. Nat. Geosci. 15, 97–105. https://doi.org/10.1038/s41561-021-00889-9

Benettin, P., Bertuzzo, E., 2018. *tran*-SAS v1.0: a numerical model to compute catchment-scale hydrologic transport using StorAge Selection functions. Geosci. Model Dev. 11, 1627–1639. https://doi.org/10.5194/gmd-11-1627-2018

Benettin P., Kirchner J.W., Rinaldo A., Botter G., 2015. Modeling chloride transport using travel time distributions at Plynlimon, Wales. Water Resour. Res. 51, 3259–3276. https://doi.org/10.1002/2014WR016600

Benettin, P., Rinaldo, A., Botter, G., 2015. Tracking residence times in hydrological systems: forward and backward formulations. Hydrol. Process. 29, 5203–5213. https://doi.org/10.1002/hyp.10513

Benettin, P., Rodriguez, N.B., Sprenger, M., Kim, M., Klaus, J., Harman, C.J., van der Velde, Y., Hrachowitz, M., Botter, G., McGuire, K.J., Kirchner, J.W., Rinaldo, A., McDonnell, J.J., 2022. Transit Time Estimation in Catchments: Recent Developments and Future Directions. Water Resour. Res. 58, e2022WR033096. https://doi.org/10.1029/2022WR033096

Benettin, P., Soulsby, C., Birkel, C., Tetzlaff, D., Botter, G., Rinaldo, A., 2017. Using SAS functions and high-resolution isotope data to unravel travel time distributions in headwater catchments. Water Resour. Res. 53, 1864–1878. https://doi.org/10.1002/2016WR020117

Blöschl, G., Bierkens, M.F.P., Chambel, A., Cudennec, C., Destouni, G., Fiori, A., Kirchner, J.W., McDonnell, J.J., Savenije, H.H.G., Sivapalan, M., Stumpp, C., Toth, E., Volpi, E., Carr, G., Lupton, C., Salinas, J., Széles, B., Viglione, A., Aksoy, H., Allen, S.T., Amin, A., Andréassian, V., Arheimer, B., Aryal, S.K., Baker, V., Bardsley, E., Barendrecht, M.H., Bartosova, A., Batelaan, O., Berghuijs, W.R., Beven, K., Blume, T., Bogaard, T., Amorim, P.B. de, Böttcher, M.E., Boulet, G., Breinl, K., Brilly, M., Brocca, L., Buytaert, W., Castellarin, A., Castelletti, A., Chen, X., Chen, Yangbo, Chen, Yuanfang, Chifflard, P., Claps, P., Clark, M.P., Collins, A.L., Croke, B., Dathe, A., David, P.C., Barros, F.P.J. de, Rooij, G. de, Baldassarre, G.D., Driscoll, J.M., Duethmann, D., Dwivedi, R., Eris, E., Farmer, W.H., Feiccabrino, J., Ferguson, G., Ferrari, E., Ferraris, S., Fersch, B., Finger, D., Foglia, L., Fowler, K., Gartsman, B., Gascoin, S., Gaume, E., Gelfan, A., Geris, J., Gharari, S., Gleeson, T., Glendell, M., Bevacqua, A.G., González-Dugo, M.P., Grimaldi, S., Gupta, A.B., Guse, B., Han, D., Hannah, D., Harpold, A., Haun, S., Heal, K., Helfricht, K., Herrnegger, M., Hipsey, M., Hlaváčiková, H., Hohmann, C., Holko, L., Hopkinson, C., Hrachowitz, M., Illangasekare, T.H., Inam, A., Innocente, C., Istanbulluoglu, E., Jarihani, B., Kalantari, Z., Kalvans, A., Khanal, S., Khatami, S., Kiesel, J., Kirkby, M., Knoben, W., Kochanek, K., Kohnová, S., Kolechkina, A., Krause, S., Kreamer, D., Kreibich, H., Kunstmann, H., Lange, H., Liberato, M.L.R., Lindquist, E., Link, T., Liu, J., Loucks, D.P., Luce, C., Mahé, G., Makarieva, O., Malard, J., Mashtayeva, S., Maskey, S., Mas-Pla, J., Mavrova-Guirguinova, M., Mazzoleni, M., Mernild, S., Misstear, B.D., Montanari, A., Müller-Thomy, H., Nabizadeh, A., Nardi, F., Neale, C., Nesterova, N., Nurtaev, B., Odongo, V.O., Panda, S., Pande, S., Pang, Z., Papacharalampous, G., Perrin, C., Pfister, L., Pimentel, R., Polo, M.J., Post, D., Sierra, C.P., Ramos, M.-H., Renner, M., Reynolds, J.E., Ridolfi, E., Rigon, R., Riva, M., Robertson, D.E., Rosso, R., Roy, T., Sá, J.H.M., Salvadori, G., Sandells, M., Schaefli, B., Schumann, A., Scolobig, A., Seibert, J., Servat, E., Shafiei, M., Sharma, A., Sidibe, M., Sidle, R.C., Skaugen, T., Smith, H., Spiessl, S.M., Stein, L., Steinsland, I., Strasser, U., Su, B., Szolgay, J., Tarboton, D., Tauro, F., Thirel, G., Tian, F., Tong, R., Tussupova, K., Tyralis, H., Uijlenhoet, R., Beek, R. van, Ent, R.J. van der, Ploeg, M. van der, Loon, A.F.V., Meerveld, I. van, Nooijen, R. van, Oel, P.R. van, Vidal, J.-P., Freyberg, J. von, Vorogushyn, S., Wachniew, P., Wade, A.J., Ward, P., Westerberg, I.K., White, C., Wood, E.F., Woods, R., Xu, Z., Yilmaz, K.K., Zhang, Y., 2019. Twenty-three unsolved problems in hydrology (UPH) – a community perspective. Hydrol. Sci. J. 64, 1141–1158. https://doi.org/10.1080/02626667.2019.1620507

Botter, G., Bertuzzo, E., Rinaldo, A., 2011. Catchment residence and travel time distributions: The master equation: CATCHMENT RESIDENCE TIMES. Geophys. Res. Lett. 38, n/a-n/a. https://doi.org/10.1029/2011GL047666

Botter, G., Bertuzzo, E., Rinaldo, A., 2010. Transport in the hydrologic response: Travel time distributions, soil moisture dynamics, and the old water paradox: A THEORY OF TRANSPORT IN THE HYDROLOGIC RESPONSE. Water Resour. Res. 46. https://doi.org/10.1029/2009WR008371

Bowes M.J., Jarvie H.P., Halliday S.J., Skeffington R.A., Wade A.J., Loewenthal M., Gozzard E., Newman J.R., Palmer-Felgate E.J., 2015. Characterising phosphorus and nitrate inputs to a rural river using high-frequency concentration–flow relationships. Sci. Total Environ. 511, 608–620. https://doi.org/10.1016/j.scitotenv.2014.12.086

Chang, S.Y., Zhang, Q., Byrnes, D.K., Basu, N.B., Meter, K.J.V., 2021. Chesapeake legacies: the importance of legacy nitrogen to improving Chesapeake Bay water quality. Environ. Res. Lett. 16, 085002. https://doi.org/10.1088/1748-9326/ac0d7b

Chen, D., Hu, M., Guo, Y., Wang, J., Huang, H., Dahlgren, R.A., 2017. Long-term (1980–2010) changes in cropland phosphorus budgets, use efficiency and legacy pools across townships in the Yongan watershed, eastern China. Agric. Ecosyst. Environ. 236, 166–176. https://doi.org/10.1016/j.agee.2016.12.003

Chen, L., Li, J., Xu, J., Liu, G., Wang, W., Jiang, J., Shen, Z., 2022. New framework for nonpoint source pollution management based on downscaling priority management areas. J. Hydrol. 606, 127433. https://doi.org/10.1016/j.jhydrol.2022.127433

Chen, S., Chen, L., Liu, X., Pan, Y., Zhou, F., Guo, J., Huang, T., Chen, F., Shen, Z., 2022. Unexpected nitrogen flow and water quality change due to varying atmospheric deposition. J. Hydrol. 609, 127679. https://doi.org/10.1016/j.jhydrol.2022.127679

Chesapeake Progress, n.d. 2017 and 2025 Watershed Implementation Plans (WIPs) [WWW Document]. Chesap. Prog. URL https://www.chesapeakeprogress.com/clean-water/watershed-implementation-plans (accessed 3.2.23).

Danesh-Yazdi, M., Klaus, J., Condon, L.E., Maxwell, R.M., 2018. Bridging the gap between numerical solutions of travel time distributions and analytical storage selection functions. Hydrol. Process. 32, 1063–1076. https://doi.org/10.1002/hyp.11481

Davies, J., Beven, K., Rodhe, A., Nyberg, L., Bishop, K., 2013. Integrated modeling of flow and residence times at the catchment scale with multiple interacting pathways. Water Resour. Res. 49, 4738–4750. https://doi.org/10.1002/wrcr.20377

Dupas, R., Ehrhardt, S., Musolff, A., Fovet, O., Durand, P., 2020. Long-term nitrogen retention and transit time distribution in agricultural catchments in western France. Environ. Res. Lett. 15, 115011. https://doi.org/10.1088/1748-9326/abbe47

Ehrhardt, S., Ebeling, P., Dupas, R., Kumar, R., Fleckenstein, J.H., Musolff, A., 2021. Nitrate Transport and Retention in Western European Catchments Are Shaped by Hydroclimate and Subsurface Properties. Water Resour. Res. 57, e2020WR029469. https://doi.org/10.1029/2020WR029469

Ejigu, M.T., 2021. Overview of water quality modeling. Cogent Eng. 8, 1891711. https://doi.org/10.1080/23311916.2021.1891711

Engdahl, N.B., Maxwell, R.M., 2015. Quantifying changes in age distributions and the hydrologic balance of a high-mountain watershed from climate induced variations in recharge. J. Hydrol. 522, 152–162. https://doi.org/10.1016/j.jhydrol.2014.12.032

Fowler K.J.A., Coxon G., Freer J.E., Knoben W.J.M., Peel M.C., Wagener T., Western A.W., Woods R.A., Zhang L., 2021. Towards more realistic runoff projections by removing limits on simulated soil moisture deficit. J. Hydrol. 600, 126505. https://doi.org/10.1016/j.jhydrol.2021.126505

Fu B., Merritt W.S., Croke B.F.W., Weber T.R., Jakeman A.J., 2019. A review of catchment-scale water quality and erosion models and a synthesis of future prospects. Environ. Model. Softw. 114, 75–97. https://doi.org/10.1016/j.envsoft.2018.12.008

Godsey, S.E., Kirchner, J.W., Clow, D.W., 2009. Concentration–discharge relationships reflect chemostatic characteristics of US catchments. Hydrol. Process. 23, 1844–1864. https://doi.org/10.1002/hyp.7315

Gupta, H.V., Kling, H., Yilmaz, K.K., Martinez, G.F., 2009. Decomposition of the mean squared error and NSE performance criteria: Implications for improving hydrological modelling. J. Hydrol. 377, 80–91. https://doi.org/10.1016/j.jhydrol.2009.08.003

Harman, C.J., 2015. Time-variable transit time distributions and transport: Theory and application to storage-dependent transport of chloride in a watershed. Water Resour. Res. 51, 1–30. https://doi.org/10.1002/2014WR015707

Heidbüchel, I., Troch, P.A., Lyon, S.W., 2013. Separating physical and meteorological controls of variable transit times in zero-order catchments. Water Resour. Res. 49, 7644–7657. https://doi.org/10.1002/2012WR013149

Heidbüchel, I., Yang, J., Musolff, A., Troch, P., Ferré, T., Fleckenstein, J.H., 2019. On the shape of forward transit time distributions in low-order catchments (preprint). Catchment hydrology/Modelling approaches. https://doi.org/10.5194/hess-2019-440

Hesser, F.B., Franko, U., Rode, M., 2010. Spatially Distributed Lateral Nitrate Transport at the Catchment Scale. J. Environ. Qual. 39, 193–203. https://doi.org/10.2134/jeq2009.0031

Hrachowitz, M., Benettin, P., Breukelen, B.M. van, Fovet, O., Howden, N.J.K., Ruiz, L., Velde, Y. van der, Wade, A.J., 2016. Transit times-the link between hydrology and water quality at the catchment scale: Linking hydrology and transit times. Wiley Interdiscip. Rev. Water 3, 629–657. https://doi.org/10.1002/wat2.1155

Hrachowitz, M., Savenije, H., Bogaard, T.A., Tetzlaff, D., Soulsby, C., 2013. What can flux tracking teach us about water age distribution patterns and their temporal dynamics? Hydrol. Earth Syst. Sci. 17, 533–564. https://doi.org/10.5194/hess-17-533-2013

Hrachowitz, M., Soulsby, C., Tetzlaff, D., Malcolm, I.A., Schoups, G., 2010. Gamma distribution models for transit time estimation in catchments: Physical interpretation of parameters and implications for time-variant transit time assessment. Water Resour. Res. 46. https://doi.org/10.1029/2010WR009148

Jing M., Kumar R., Attinger S., Li Q., Lu C., Heße F., 2021. Assessing the contribution of groundwater to catchment travel time distributions through integrating conceptual flux tracking with explicit Lagrangian particle tracking. Adv. Water Resour. 149, 103849. https://doi.org/10.1016/j.advwatres.2021.103849

Kim, M., Volkmann, T.H.M., Wang, Y., Meira Neto, A.A., Matos, K., Harman, C.J., Troch, P.A., 2022. Direct Observation of Hillslope Scale StorAge Selection Functions in Experimental Hydrologic Systems: Geomorphologic Structure and Preferential Discharge of Old Water. Water Resour. Res. 58, e2020WR028959. https://doi.org/10.1029/2020WR028959

Kim, N.W., Chung, I.M., Won, Y.S., Arnold, J.G., 2008. Development and application of the integrated SWAT–MODFLOW model. J. Hydrol. 356, 1–16. https://doi.org/10.1016/j.jhydrol.2008.02.024

Kirchner, J.W., 2006. Getting the right answers for the right reasons: Linking measurements, analyses, and models to advance the science of hydrology. Water Resour. Res. 42. https://doi.org/10.1029/2005WR004362

Kirchner, J.W., 2003. A double paradox in catchment hydrology and geochemistry. Hydrol. Process. 17, 871–874. https://doi.org/10.1002/hyp.5108

Kirchner, J.W., Feng, X., Neal, C., 2000. Fractal stream chemistry and its implications for contaminant transport in catchments. Nature 403, 524–527. https://doi.org/10.1038/35000537

Knoben, W.J.M., Freer, J.E., Woods, R.A., 2019. Technical note: Inherent benchmark or not? Comparing Nash-Sutcliffe and Kling-Gupta efficiency scores (preprint). Catchment hydrology/Modelling approaches. https://doi.org/10.5194/hess-2019-327

Kumar, R., Heße, F., Rao, P.S.C., Musolff, A., Jawitz, J.W., Sarrazin, F., Samaniego, L., Fleckenstein, J.H., Rakovec, O., Thober, S., Attinger, S., 2020. Strong hydroclimatic controls on vulnerability to subsurface nitrate contamination across Europe. Nat. Commun. 11, 6302. https://doi.org/10.1038/s41467-020-19955-8

Liu, D., 2020. A rational performance criterion for hydrological model. J. Hydrol. 590, 125488. https://doi.org/10.1016/j.jhydrol.2020.125488

Liu, R., Xu, F., Zhang, P., Yu, W., Men, C., 2016. Identifying non-point source critical source areas based on multi-factors at a basin scale with SWAT. J. Hydrol. 533, 379–388. https://doi.org/10.1016/j.jhydrol.2015.12.024

Lutz, S.R., Ebeling, P., Musolff, A., Van Nguyen, T., Sarrazin, F.J., Van Meter, K.J., Basu, N.B., Fleckenstein, J.H., Attinger, S., Kumar, R., 2022. Pulling the rabbit out of the hat: Unravelling hidden nitrogen legacies in CATCHMENT-SCALE water quality models. Hydrol. Process. 36. https://doi.org/10.1002/hyp.14682

Maloszewski, P., Zuber, A., 1993. Principles and practice of calibration and validation of mathematical models for the interpretation of environmental tracer data in aquifers. Adv. Water Resour. 16, 173–190. https://doi.org/10.1016/0309-1708(93)90036-F

Maloszewski, P., Zuber, A., 1982. Determining the turnover time of groundwater systems with the aid of environmental tracers: 1. Models and their applicability. J. Hydrol. 57, 207–231. https://doi.org/10.1016/0022-1694(82)90147-0

Maxwell, R.M., Condon, L.E., Danesh-Yazdi, M., Bearup, L.A., 2019. Exploring source water mixing and transient residence time distributions of outflow and evapotranspiration with an integrated hydrologic model and Lagrangian particle tracking approach. Ecohydrology 12, e2042. https://doi.org/10.1002/eco.2042

McDonnell, J.J., McGuire, K., Aggarwal, P., Beven, K.J., Biondi, D., Destouni, G., Dunn, S., James, A., Kirchner, J., Kraft, P., Lyon, S., Maloszewski, P., Newman, B., Pfister, L., Rinaldo, A., Rodhe, A., Sayama, T., Seibert, J., Solomon, K., Soulsby, C., Stewart, M., Tetzlaff, D., Tobin, C., Troch, P., Weiler, M., Western, A., Wörman, A., Wrede, S., 2010. How old is streamwater? Open questions in catchment transit time conceptualization, modelling and analysis. Hydrol. Process. 24, 1745–1754. https://doi.org/10.1002/hyp.7796

McDowell, R.W., Simpson, Z.P., Ausseil, A.G., Etheridge, Z., Law, R., 2021. The implications of lag times between nitrate leaching losses and riverine loads for water quality policy. Sci. Rep. 11, 16450. https://doi.org/10.1038/s41598-021-95302-1

McGuire, K.J., McDonnell, J.J., 2006. A review and evaluation of catchment transit time modeling. J. Hydrol. 330, 543–563. https://doi.org/10.1016/j.jhydrol.2006.04.020

McGuire, K.J., Weiler, M., McDonnell, J.J., 2007. Integrating tracer experiments with modeling to assess runoff processes and water transit times. Adv. Water Resour. 30, 824–837. https://doi.org/10.1016/j.advwatres.2006.07.004

Meira Neto, A.A., Kim, M., Troch, P.A., 2022. Physical Interpretation of Time-Varying StorAge Selection Functions in a Bench-Scale Hillslope Experiment via Geophysical Imaging of Ages of Water. Water Resour. Res. 58, e2021WR030950. https://doi.org/10.1029/2021WR030950

Meter, K.J.V., Cappellen, P.V., Basu, N.B., 2018. Legacy nitrogen may prevent achievement of water quality goals in the Gulf of Mexico. Science 360, 427–430. https://doi.org/10.1126/science.aar4462

Moriasi, D.N., Arnold, J.G., Liew, M.W.V., Bingner, R.L., Harmel, R.D., Veith, T.L., 2007. Model Evaluation Guidelines for Systematic Quantification of Accuracy in Watershed Simulations. Trans. ASABE 50, 885–900. https://doi.org/10.13031/2013.23153

Moriasi, D.N., Gitau, M.W., Pai, N., Daggupati, P., 2015. Hydrologic and Water Quality Models: Performance Measures and Evaluation Criteria. Trans. ASABE 58, 1763–1785. https://doi.org/10.13031/trans.58.10715

Musolff A., Schmidt C., Selle B., Fleckenstein J.H., 2015. Catchment controls on solute export. Adv. Water Resour. 86, 133–146. https://doi.org/10.1016/j.advwatres.2015.09.026

Nangia V., Gowda P.H., Mulla D.J., Sands G.R., 2008. Water Quality Modeling of Fertilizer Management Impacts on Nitrate Losses in Tile Drains at the Field Scale. J. Environ. Qual. 37, 296–307. https://doi.org/10.2134/jeq2007.0224

Narula, K.K., Gosain, A.K., 2013. Modeling hydrology, groundwater recharge and non-point nitrate loadings in the Himalayan Upper Yamuna basin. Sci. Total Environ. 468-469 Suppl, S102-116. https://doi.org/10.1016/j.scitotenv.2013.01.022

Nash, J.E., Sutcliffe, J.V., 1970. River flow forecasting through conceptual models part I — A discussion of principles. J. Hydrol. 10, 282–290. https://doi.org/10.1016/0022-1694(70)90255-6

Neira, J.M.T., 2019. Revisiting the concentration-discharge (C-Q) relationships with high-frequency measurements. Sorbonne Université.

Neitsch, S.L., Arnold, J.G., Kiniry, J.R., Williams, J.R., 2011. Soil and Water Assessment Tool Theoretical Documentation (Version 2009) (Texas Water Resources Institute Technical Report No. TR-406). Texas A&M University, Texas.

Nguyen, T.V., Dietrich, J., Dang, T.D., Tran, D.A., Van Doan, B., Sarrazin, F.J., Abbaspour, K., Srinivasan, R., 2022a. An interactive graphical interface tool for parameter calibration, sensitivity analysis, uncertainty analysis, and visualization for the Soil and Water Assessment Tool. Environ. Model. Softw. 156, 105497. https://doi.org/10.1016/j.envsoft.2022.105497

Nguyen, T.V., Kumar, R., Lutz, S.R., Musolff, A., Yang, J., Fleckenstein, J.H., 2021. Modeling Nitrate Export From a Mesoscale Catchment Using StorAge Selection Functions. Water Resour. Res. 57, e2020WR028490. https://doi.org/10.1029/2020WR028490

Nguyen, T.V., Kumar, R., Musolff, A., Lutz, S.R., Sarrazin, F., Attinger, S., Fleckenstein, J.H., 2022b. Disparate Seasonal Nitrate Export From Nested Heterogeneous Subcatchments Revealed With StorAge Selection Functions. Water Resour. Res. 58, e2021WR030797. https://doi.org/10.1029/2021WR030797

Nguyen, V.T., Dietrich, J., Uniyal, B., 2020. Modeling interbasin groundwater flow in karst areas: Model development, application, and calibration strategy. Environ. Model. Softw. 124, 104606. https://doi.org/10.1016/j.envsoft.2019.104606

Niemi, A.J., 1977. Residence time distributions of variable flow processes. Int. J. Appl. Radiat. Isot. 28, 855–860. https://doi.org/10.1016/0020-708X(77)90026-6

Qi, J., Li, S., Li, Q., Xing, Z., Bourque, C.P.-A., Meng, F.-R., 2016. A new soil-temperature module for SWAT application in regions with seasonal snow cover. J. Hydrol. 538, 863–877. https://doi.org/10.1016/j.jhydrol.2016.05.003

Queloz, P., Carraro, L., Benettin, P., Botter, G., Rinaldo, A., Bertuzzo, E., 2015. Transport of fluorobenzoate tracers in a vegetated hydrologic control volume: 2. Theoretical inferences and modeling. Water Resour. Res. 51, 2793–2806. https://doi.org/10.1002/2014WR016508

Rakovec, O., Samaniego, L., Hari, V., Markonis, Y., Moravec, V., Thober, S., Hanel, M., Kumar, R., 2022. The 2018–2020 Multi-Year Drought Sets a New Benchmark in Europe. Earths Future 10, e2021EF002394. https://doi.org/10.1029/2021EF002394

Remondi, F., Kirchner, J.W., Burlando, P., Fatichi, S., 2018. Water Flux Tracking With a Distributed Hydrological Model to Quantify Controls on the Spatio-temporal Variability of Transit Time Distributions. Water Resour. Res. 54, 3081–3099. https://doi.org/10.1002/2017WR021689

Renée Brooks, J., Barnard, H.R., Coulombe, R., McDonnell, J.J., 2010. Ecohydrologic separation of water between trees and streams in a Mediterranean climate. Nat. Geosci. 3, 100–104. https://doi.org/10.1038/ngeo722

Rinaldo, A., Benettin, P., Harman, C.J., Hrachowitz, M., McGuire, K.J., Velde, Y. van der, Bertuzzo, E., Botter, G., 2015. Storage selection functions: A coherent framework for quantifying how catchments store and release water and solutes: ON STORAGE SELECTION FUNCTIONS. Water Resour. Res. 51, 4840–4847. https://doi.org/10.1002/2015WR017273

Rinaldo, A., Marani, A., 1987. Basin scale model of solute transport. Water Resour. Res. 23, 2107–2118. https://doi.org/10.1029/WR023i011p02107

Rodriguez, N.B., Klaus, J., 2019. Catchment Travel Times From Composite StorAge Selection Functions Representing the Superposition of Streamflow Generation Processes. Water Resour. Res. 55, 9292–9314. https://doi.org/10.1029/2019WR024973

Rodriguez, N.B., Pfister, L., Zehe, E., Klaus, J., 2021. A comparison of catchment travel times and storage deduced from deuterium and tritium tracers using StorAge Selection functions. Hydrol. Earth Syst. Sci. 25, 401–428. https://doi.org/10.5194/hess-25-401-2021

Rodriguez, N.B., Pfister, L., Zehe, E., Klaus, J., 2019. Testing the truncation of travel times with StorAge Selection functions using deuterium and tritium as tracers (preprint). Catchment hydrology/Modelling approaches. https://doi.org/10.5194/hess-2019-501

Sinha, S., Rode, M., Borchardt, D., 2016. Examining runoff generation processes in the Selke catchment in central Germany: Insights from data and semi-distributed numerical model. J. Hydrol. Reg. Stud. 7, 38–54. https://doi.org/10.1016/j.ejrh.2016.06.002

Smith, A. A., Tetzlaff, D., Soulsby, C., 2018. On the Use of StorAge Selection Functions to Assess Time-Variant Travel Times in Lakes. Water Resour. Res. 54, 5163–5185. https://doi.org/10.1029/2017WR021242

Smith, Aaron A., Tetzlaff, D., Soulsby, C., 2018. Using StorAge Selection functions to quantify ecohydrological controls on the time-variant age of evapotranspiration, soil water, and recharge (preprint). Vadose Zone Hydrology/Modelling approaches. https://doi.org/10.5194/hess-2018-57

Sprenger, M., Stumpp, C., Weiler, M., Aeschbach, W., Allen, S.T., Benettin, P., Dubbert, M., Hartmann, A., Hrachowitz, M., Kirchner, J.W., McDonnell, J.J., Orlowski, N., Penna, D., Pfahl, S., Rinderer, M., Rodriguez, N., Schmidt, M., Werner, C., 2019. The Demographics of Water: A Review of Water Ages in the Critical Zone. Rev. Geophys. 57, 800–834. https://doi.org/10.1029/2018RG000633

Van Vliet, M.T.H., Thorslund, J., Strokal, M., Hofstra, N., Flörke, M., Ehalt Macedo, H., Nkwasa, A., Tang, T., Kaushal, S.S., Kumar, R., Van Griensven, A., Bouwman, L., Mosley, L.M., 2023. Global river water quality under climate change and hydroclimatic extremes. Nat. Rev. Earth Environ. https://doi.org/10.1038/s43017-023-00472-3

Velde, Y. van der, Rooij, G.H. de, Rozemeijer, J.C., Geer, F.C. van, Broers, H.P., 2010. Nitrate response of a lowland catchment: On the relation between stream concentration and travel time distribution dynamics: NITRATE RESPONSE OF A LOWLAND CATCHMENT. Water Resour. Res. 46. https://doi.org/10.1029/2010WR009105

Velde, Y. van der, Torfs, P.J.J.F., Zee, S.E.A.T.M. van der, Uijlenhoet, R., 2012. Quantifying catchment-scale mixing and its effect on time-varying travel time distributions: QUANTIFYING CATCHMENT-SCALE MIXING. Water Resour. Res. 48. https://doi.org/10.1029/2011WR011310

Weill, S., Lesparre, N., Jeannot, B., Delay, F., 2019. Variability of Water Transit Time Distributions at the Strengbach Catchment (Vosges Mountains, France) Inferred Through Integrated Hydrological Modeling and Particle Tracking Algorithms. Water 11, 2637. https://doi.org/10.3390/w11122637

Wen H., Brantley S.L., Davis K.J., Duncan J.M., Li L., 2021. The Limits of Homogenization: What Hydrological Dynamics can a Simple Model Represent at the Catchment Scale? Water Resour. Res. 57, e2020WR029528. https://doi.org/10.1029/2020WR029528

Winter, C., Tarasova, L., Lutz, S.R., Musolff, A., Kumar, R., Fleckenstein, J.H., 2022. Explaining the Variability in High-Frequency Nitrate Export Patterns Using Long-Term Hydrological Event Classification. Water Resour. Res. 58, e2021WR030938. https://doi.org/10.1029/2021WR030938

Yang, J., Heidbüchel, I., Musolff, A., Reinstorf, F., Fleckenstein, J.H., 2018. Exploring the Dynamics of Transit Times and Subsurface Mixing in a Small Agricultural Catchment. Water Resour. Res. 54, 2317–2335. https://doi.org/10.1002/2017WR021896

Yang, J., Heidbüchel, I., Musolff, A., Xie, Y., Lu, C., Fleckenstein, J.H., 2021. Using nitrate as a tracer to constrain age selection preferences in catchments with strong seasonality. J. Hydrol. 603, 126889. https://doi.org/10.1016/j.jhydrol.2021.126889

Yang, X., Jomaa, S., Zink, M., Fleckenstein, J.H., Borchardt, D., Rode, M., 2018. A New Fully Distributed Model of Nitrate Transport and Removal at Catchment Scale. Water Resour. Res. 54, 5856–5877. https://doi.org/10.1029/2017WR022380

Yang, X., Rode, M., Jomaa, S., Merbach, I., Tetzlaff, D., Soulsby, C., Borchardt, D., 2022. Functional Multi-Scale Integration of Agricultural Nitrogen-Budgets Into Catchment Water Quality Modeling. Geophys. Res. Lett. 49, e2021GL096833. https://doi.org/10.1029/2021GL096833

Zhang, D., Chen, X., Yao, H., Lin, B., 2015. Improved calibration scheme of SWAT by separating wet and dry seasons. Ecol. Model. 301, 54–61. https://doi.org/10.1016/j.ecolmodel.2015.01.018

Zhang, X., Yang, X., Jomaa, S., Rode, M., 2020. Analyzing impacts of seasonality and landscape gradient on event-scale nitrate-discharge dynamics based on nested high-frequency monitoring. J. Hydrol. 591, 125585. https://doi.org/10.1016/j.jhydrol.2020.125585

Zhang, Z., Chen, X., Cheng, Q. bo, Soulsby, C., 2020. Characterising the variability of transit time distributions and young water fractions in a karst catchment using flux tracking. https://doi.org/10.22541/au.157851585.50807186

Zhang, Z., Chen, X., Cheng, Q., Soulsby, C., 2021. Using StorAge Selection (SAS) functions to understand flow paths and age distributions in contrasting karst groundwater systems. J. Hydrol. 602, 126785. https://doi.org/10.1016/j.jhydrol.2021.126785